HIGH TEMPERATURE PROCESSABLE NANOFIBROUS INTERLAYERS FOR COMPOSITE STRUCTURES

by

Ayça ÜRKMEZ

Submitted to Graduate School of Engineering and Natural Sciences

in partial fulfillment of

the requirements for the degree of

Master of Science

Sabancı University

June, 2015

HIGH TEMPERATURE PROCESSABLE NANOFIBROUS INTERLAYERS FOR COMPOSITE STRUCTURES

APPROVED BY:

Assoc. Prof. Dr. Melih Papila..

(Thesis Advisor)

Prof. Dr. Ali Rana Atılgan..

Assoc. Prof. Dr. Nuri Ersoy..

DATE OF APPROVAL: 19/6/2015

La Vita è Bella

To my beloved father

"Babama..."

HIGH TEMPERATURE PROCESSABLE NANOFIBROUS INTERLAYERS FOR COMPOSITE STRUCTURES

Ayça Ürkmez

MAT, Master of Science Thesis, 2015

Thesis Supervisor: Assoc. Prof. Dr. Melih Papila

Keywords: composite materials, nanofiber, interlayer, cross-linking, thermal behaviour

Abstract

Nano-engineering of composite materials is an expanding research field, thanks to emerging manufacturing techniques and intriguing properties of nano-scale materials. It requires both "multi-disciplinary" and "multi-scaled" research insight for achieving the ultimate goal of superior material properties preferably with multifunctionality. Enhancing the mechanical properties such as toughening is arguably the most common interest.

Interlayer toughening of structural composite materials is one of the several toughening mechanisms where interlaminar region, being one of the weakest links in composite structures, is at focus for the material solution developed here. Nano-interlayer toughening strategy thus aims to integrate nano-scaled reinforcements to interlaminar regions in order to improve the mechanical performance with minimum weight addition. Following this strategy, this thesis work firstly investigates the effect of glass transition temperature on the morphology of electrospun P(St-co-GMA) nanofibers which are proven to be a potential candidate for interlayer toughening in composite materials thanks to their epoxy compatibility. Secondly it offers a unique

way to undisrupted electrospinning of these nanofibers in the presence of crosslinking agents. The goal is to achieve in-situ crosslinking at heat stimuli consistent with typical cure cycles of advanced polymeric composites. The thesis work is divided into two subsections:

Heat Stimuli Self Crosslinking of Electrospun Nanofibers: Stimuli-Self – Crosslinking ability is introduced to P(St-co-GMA) nanofibers by the addition of Phtalic Anhydride (PA) as cross-linking agent and tributylamine (TBA) as the catalyst. Heat activated crosslinking procedure enables the manufacturing of cross-linkable nanofibers through electrospinning at room temperature without any rheological problems. A complete cross-linking event is characterized by co-use of FT-IR analysis focusing the consumption of PA and disappearance of available active sites in copolymer and swelling tests. Glass transition temperature of self-cross-linked copolymers increases by 30ºC without any post chemical treatments required, elevated temperature effect on the nanofiber morphology change before and after crosslinking is determined by SEM analysis.

In-situ crosslinakable nanofibers for structural composites: The crosslinking recipe optimized in the first part is offered for the incorporation of polymeric nanofibrous interlayers into structural composites where high temperature curing cycle is needed. The hypothesis is that heat stimuli-self crosslinking enables a homogenous crosslinking regime both for nanofibers and epoxy matrix itself during curing which results in better mechanical performance. Following this motivation an example case is demonstrated where stimuli-self-crosslinkable P(St-co-GMA)/PA-TBA nanofibrous interlayers are added to carbon/epoxy prepreg composites cured at 135°C. Interlayered laminates are subjected to three-point bending and mode II fracture toughness tests (end-notched flexure-ENF). Mechanical test results are accompanied by cross-sectional and fracture surface microscopy analysis through Scanning Electron Microscopy (SEM). As a result of mechanical tests a significant increase in resistance against mode II delamination (80%) and flexural strength (15%) with precisely no weight penalty was observed.

YÜKSEK SICAKLIK DAYANIMLI NANOLİF ARAYÜZLERİN KOMPOZİT YAPILARA UYGULANMASI

Ayça Ürkmez

MAT, Yüksek Lisans Tezi, 2015

Tez Danışmanı: Yard. Doç. Dr. Melih Papila

Anahtar Kelimeler: kompozit malzemeler, nanolif, arayüzey, çapraz bağlanma, termal özlellik

Özet

Kompozit malzemelerin nano-boyuttaki mühendislik çalışmaları ve uygulamaları yaygınlaşmakta olan bir araştırma alanıdır. Araştırmacılar bahsedilen mühendislik çalışmalarını yeni üretim yöntemleri ve son zamanlarda keşfedilen ve umut verici özelliklere sahip olan nano-boyuttaki malzemelerle bir bütün olarak ele alıp bunlar üzerine yoğunlaşmaktadır. Malzeme özellikleri farklı zaman ve boyut ölçeklerinde hesaplanan nano-mühendislik ürünü kompozit malzemeler "disiplinler arası" ve "çok-ölçekli" bir araştırma anlayışı gerektirmektedir. Yapısal kompozit malzemelerde kullanılan "katmanlar arası güçlendirme" yöntemi birçok toklaştırma mekanizmasından biridir ki bu laminalar arası bölge kompozit malzemelerin en zayıf bölgesi olarak addedilmektedir ve çalışmaların odak noktasında bulunmaktadır. Nano-katmalar arası güçlendirme stratejisi, nano ölçekli takviye malzemelerinin laminalar arası bölgeye entegrasyonunu sağlayarak, mekanik performansı minimum ağırlık artışı ile arttırmayı amaçlamaktadır. Bahsedilen stratejiyi baz alarak bu tez çalışmasında, ilk olarak katmanlar arası güçlendirme potansiyeli kanıtlanmış olan P(St-co-GMA) nanofiberlerinin morfolojisi üzerinde camsı geçiş sıcaklığının etkisi gözlenmiştir. İkincil olarak da ısıl etki ile yerinde çapraz bağlanan ve içerisinde çapraz bağlayıcı ihtiva eden solüsyonların sorunsuz ve devamlı elektro-dokuması sağlanmıştır. Ayrıntılandırmak gerekirse bu tez iki alt kısım içermektedir.

Isıl etki ile kendiliğinden çapraz bağlanabilen nanoliflerin elektro-dokuması: P(St-co-GMA) nanoliflerine Stimuli-kendiliğinden-çapraz bağlanabilme özelliği, çapraz bağlayıcı (Ftalik Anhidrid) başlatıcı (Tribtilamin) eklenerek kazandırılmıştır. Sıcaklıkla aktive olan çapraz bağlanma prosedürü oda sıcaklığında her hangi bir reolojik problemle karşılaşılmaksızın nanolif üretimini mümkün kılmıştır.Çapraz bağlanma reaksiyon sonrasında ftalik anhidrid harcanmasına bağlı olarak FT-IR spektrumunda aktif uçların kopolimer içeriğindeki epoksid halkası ile bağ yaparak kaybolması ve şişme testleri ile karakterize edilmiştir. Nanoliflerin art kimyasal işlem gerekmeksizin camsı geçiş sıcaklıkları 30 ºC arttırılmıştır. Çapraz bağlanma öncesi ve sonrası morfolojik değişimler taramalı elektron mikroskobu (SEM) analizleri ile incelenmiştir.

Yerinde çapraz bağlanabilen nanoliflerin yapısal kompozitlere uygulaması: Termal stabilite çalışmalarında oluşturulan çapraz bağlanma reçetesi P(St-co-GMA) nanofibelerinin camı geçiş sıcaklıklarının aşılması gereken kürlenme prosedürüne sahip yapısal kompozitlere polimerik nanolif olarak uygulanmak üzere bir çalışma oluşturulmuştur. Hipotez stimuli-kendiliğinden-çapraz bağlanabilen nanoliflerin kürlenme sırasında hem kendi aralarında hem de kompozit içerisinde epoksi ile homojen biçimde çapraz bağlanarak geliştirilmiş mekanik özellik elde etmeyi amaçlamak olarak özetlenebilir. Bu motivasyonla stimuli-kendiliğinden-çapraz bağlanabilen P(St-co-GMA)/PA-TBA ve 150 ºC üzerinde çalışabilen nanolifleri yapısal kompozitlere arayüzey olarak uygulanarak bir deneyler serisi planlanmıştır. Arayüzeylerle katkılandırılmış yapısal kompozitler 3-nokta eğme, düz-kesme kuvvetlerine maruz bırakılmıştır. Mekanik test sonuçları enine kesit ve kırılma yüzeyleri üzerinden taramalı elektron mikroskobu ile incelenmiştir. Yapılan mekanik testlerin sonucunda görülmüştürki mod II delaminasyon mukavemetinde % 80’ e varan bir artış gözlenmiş bununla beraber eğilme mukavemetinde % 15 oranında iyileşme gözlenmiştir ve bu sonuçlar belirgin bir ağırlık artışı olmadan sağlanmıştır.

Acknowledgements

Though only my name appears on the cover of this dissertation, a great many people have contributed to its production. I owe my gratitude to all those people who have made this dissertation possible and because of whom my graduate experience has been one that I will cherish forever.

First and foremost I would like to express my heartfelt gratitude to my supervisor Assoc. Prof Dr Melih Papila for his academic guidance, continuous support and encouragement throughout this project. He always illuminated me when I had problems and difficulties during the experimental and composing works of my MSc.

I would also like to thank Prof. Dr. Ali Rana Atılgan and Assoc. Prof. Dr. Nuri Ersoy for serving as defense committee members also for their valuable comments and reviews.

I am thankful to TUBITAK for providing me scholarship and project funding (TUBITAK 213M542) during my thesis.

I would to extend my sincere thanks to Dr. Kılıçaslan Noyan Bayraktar for being a guide to me in every division in life.

I also would like to extend my sincere thanks to Prof. Dr. Mehmet Ali Gülgün for his encouragement and support.

I want to also express my appreciation towards all my present and former colleagues at the division of Material Science & Engineering for the nice working environment, which has made my time at the SU most pleasant. My deepest gratitude goes to my dearest colleague Kaan Bilge for his endless help, input, and friendship throughout my MSc years. I would like to thank our group members Bengisu Yılmaz and Farzin Javanshour for their support. I would like also thank to Elif Özden Yenigün, Eren Şimşek, Mustafa Baysal and Turgay Gönül for their help during my research. Though I cannot possibly list them all, I offer my special thanks to all SU members.

I would like to thank Tuğçe Akkaş for her kind friendship and all the laughter we shared.

I would like to extend my sincere thanks to Dilay Ünal, whom I can always share my feelings and secrets for her endless help as a sister till the very first day of the SU.

I would like also to thank Güliz İnan Akmehmet for sharing, cheering, supporting me and most of all being a second family to me in İstanbul with her kind husband Celal.

I would like to thank Boğaç Poyraz for beautifying my life with a priceless balloon which I want to carry for the rest of my life.

Most importantly, none of this would have been possible without the love and patience of my family. My immediate family has been a constant source of love, concern, support and strength all these years. I would like to express my heart-felt gratitude to my family, firstly a part of me my sister, who I know will always be there no matter what, to sharing all the best and worst times and converting them unforgettable memories to remember with a smile on our faces and to my brother for his existence and support mostly for his never ending energy to cheer me, especially to my father to whom this thesis dedicated to, for both being a mother and a father to us tirelessly through all these years. I would like to express my wholehearted love and thanks to my heavenly mother all the invisible love and support of her that I feel whenever I need.

TABLE OF CONTENTS

LIST OF FIGURES

LIST OF TABLES

CHAPTER 1

1.1 General Introduction

Nano-scaled engineering of composite materials is an actively broadening research field with emerging manufacturing techniques and newly discovered nano-scale materials with promising properties. Nano-engineering of composite materials both requires a "multi-disciplinary" and "a multi-scaled" research insight where material properties are evaluated at different time and length scales. Interlayer toughening of structural composite materials is one of the several toughening mechanisms where interlaminar region, being one of the weakest links in composite structures, is at focus. Nano-interlayer toughening strategy thus aims to integrate nano-scaled reinforcements to interlaminar regions aiming to improve the mechanical performance with minimum weight addition. Following this strategy, this thesis work firstly investigates the effect of glass transition temperature on the morphology of electrospun P(St-co-GMA) nanofibers which are proven to be a potential candidate for interlayer toughening in composite materials thanks to their epoxy compatibility. Secondly it offers a unique way to continuous electrospinning of these nanofibers in the presence of crosslinking agents which are to be crosslinked in-situ with heat stimuli. More specifically, the thesis is divided into two subsections:

Heat Stimuli Self Crosslinking of Electrospun Nanofibers: In structural composites nano-scaled interlayer integration to the system are expected to enhance mechanical properties at a negligible weight penalty. Nanofibers produced by the manufacturing technique electrospinning. The polymer characteristics of the electrospun nanofibers should be designed carefully to enable compatibility with the polymer matrix chemistry and stability at cure conditions. Chapter 2 investigates Stimuli-self-crosslinking ability of P(St-co-GMA) nanofibers and proposed a route for croslinking by the addition of Phthalic Anhydride (PA) as cross-linking agent and tributylamine (TBA) as the catalyst. Heat activated crosslinking procedure enabled the manufacturing of cross-linkable nanofibers through electrospinning at room temperature without any rheological problems. A complete cross-linking event is characterized by co-use of FT-IR analysis focusing the consumption of PA and disappearance of available active sites in copolymer and swelling tests. Glass transition temperature of self-cross-linked copolymers increased by 30ºC without any post chemical treatments required, elevated temperature effect on the nanofiber morphology change before and after crosslinking is determined by SEM analysis.

In-situ crosslinakable nanofibers for structural composites: Polymeric nanofiber interlayer reinforcements are considered as an encouraging strategy to toughen structural composite materials for both under in-plane and out-of-plane conditions. Thermally stable polymeric nano-fibrous interlayer morphology which is enabling wetting and interfacial compatibility with the matrix epoxy system has impact on the reinforcement performance. Therfore, investigated crosslinking recipe at the first case was offered for the application of polymeric nanofibers to structural composites where a high temperature curing above glass transition temperature of the polymer was needed. The hypothesis is that heat stimuli-self crosslinking enables a homogenous crosslinking regime both for nanofibers and epoxy matrix itself during curing which results in better mechanical performance. Following this motivation an example case is demonstrated where stimuli-self-crosslinkable P(St-co-GMA)/PA-TBA nanofibers are added to carbon/epoxy prepreg composites whose curing cycle demands 150°C application, as interlayers. Interlayered laminates are subjected to three-point bending, open-hole tensile and mode II shear tests. Mechanical test outputs are supported with cross-sectional and fracture surface microscopy analysis through Scanning Electron Microscopy.

CHAPTER 2

MATERIAL DEVELOPMENT

HEAT CONTROLLED STIMULI-SELF-CROSSLINKING OF ELECTROSPUN NANOFIBERS

2.1 Introduction

With better understanding of electrospinning process and emerging high technology systems the use of electrospun nanofibers increased significantly especially in nanocomposite [1-3], membrane [4] and structural applications [5-8] where these materials are used either as they are or in an accompanying matrix material (Nanocomposites). The key point in the application of these materials is the controllable morphology[9, 10] with usually very high surface areas [2]. Also as exemplified on the recent works of the group their chemistry is tunable to match with the matrix material which is especially important for nanocomposite applications [1]. However, fiber morphology can easily be affected from two external factors such as solvent and temperature exposure. Chemical crosslinking which is either applied externally to already electrospun nanofibers by exposure of mats to a crosslinking medium [1, 11, 12] or initiated in-situ by the introduction of crosslinking agents to polymer solutions [13-18], is an effective way to deal with these known problems. Ex-situ crosslinking herein can be classified as more conventional and direct way to achieve crosslinking by permanently changing the nanofiber chemistry. Whereas, in situ crosslinking methodology is recently a new and more controllable bulk crosslinking technique which requires an initiation event (heat, UV etc.) that is tunable according the type of application by the correct choice of polymer and crosslinking agents.

Having derived from the nanofiber compatibility works of our group on nanocomposites [1, 3]and structural composites [6-8], current work addresses to a relatively less addressed problem of T_g and its effects on P(St-co-GMA) nanofibers which is proven to be an epoxy compatible and ex-situ crosslinkable base polymer thanks to the presence of GMA groups. The thermal stability of the functional epoxide group containing P(St-co-GMA) nanofibers by implementing in-situ post-activated cross-linking mechanism for the ease and sustainability of the process. Chemical cross-linking is provided incorporation with an anhydride chemical cross-linking agent, phthalic anhydride which is react-able with epoxide group, and an appropriate tertiary amine catalyst, tributylamine, to produce stimuli-self-crosslinkable P(St-co-GMA) electrospun nanofibers and chemical crosslinking with heat treatment at intermediate temperature[19-22]. With this method, the crosslinking at room temperature was totally avoided and viscosity problem during electrospinning which is a problematic [18] is overcome. The optimization of crosslinking aiming to achieve maximum T_g and minimum morphological change upon its excession was done by altering the PA to epoxide ring mole to mole ratio from 0.5:1 to 5:1 for five different stoichiometric ratios (R) while keeping the polymer and TBA concentrations constant.

Table 2.1: Benchmarking of state-of-the-art techniques, and their main drawbacks

<table>
<tr><th colspan="3">Cross-linking type</th><th>Drawbacks</th></tr>
<tr><td><u>Ex-situ</u></td><td colspan="2">Exposing an electrospun fiber mat to a fluid cross-linking medium (liquid or vapor), or spraying a cross-linking agent thereon</td><td>- Time consuming.

- Causes substantial morphological changes.</td></tr>
<tr><td rowspan="4"><u>In-situ</u></td><td rowspan="2">Processes requiring an additional set-up</td><td>Using an UV-light source</td><td>- Restricted with UV-curable polymers.

- Requires additional equipment.</td></tr>
<tr><td>Using a dual-syringe reactive cross-linking set-up</td><td>- Additional viscosity modifiers and removal of them.

- Time consuming.</td></tr>
<tr><td>Post-electrospinning treatment</td><td>Heat treatment</td><td>- Curing temperature restrictions and related morphological changes based on the glass-transition temperature (T_g) of the polymer.</td></tr>
<tr><td colspan="2">Single step in-situ cross-linking</td><td>- Viscosity changes during electrospinning.

- Time-dependent procedure.</td></tr>
</table>

2.2 Experimental Procedure

2.2.1 Copolymer Synthesis

The purified monomers of styrene (St) and glycidylmethacrylate (GMA), solvents dimethylformamide and methanol, initiator azobisisobutyronitrile (AIBN) were purchased from Aldrich Chemical Co. Solution polymerization technique was used for copolymer poly(St-co-GMA) (see Figure 2.1) synthesis. Styrene and GMA (by mole fractions m=0.9 styrene and n=0.1 GMA) were mixed at the round bottom reaction flask contained in an ice bath. Dimetylformamide (DMF) was then added into reaction flask with a 3:2 volume proportion solvent to monomer. The initiator AIBN was then added in to monomer solvent mix and the reaction flask flushed with nitrogen.

The tube containing the dissolved monomers was then kept for 5 days in the constant temperature bath at 65˚C for the polymerization reaction. Finally, the polymer solution was poured out by drop wise into a beaker containing methanol and the methanol/polymer mixture was filtered and dried in a vacuum oven at 60˚C for 1 day. The synthesized P(St-co-GMA) copolymer structure was determined by proton magnetic resonance spectroscopy (1H-NMR). Molecular weights and polydispersities (PDI) were measured by a gel permeation chromatography (GPC) system and the molecular weight recorded as 220,000 g/mole with 1.54 PDI.

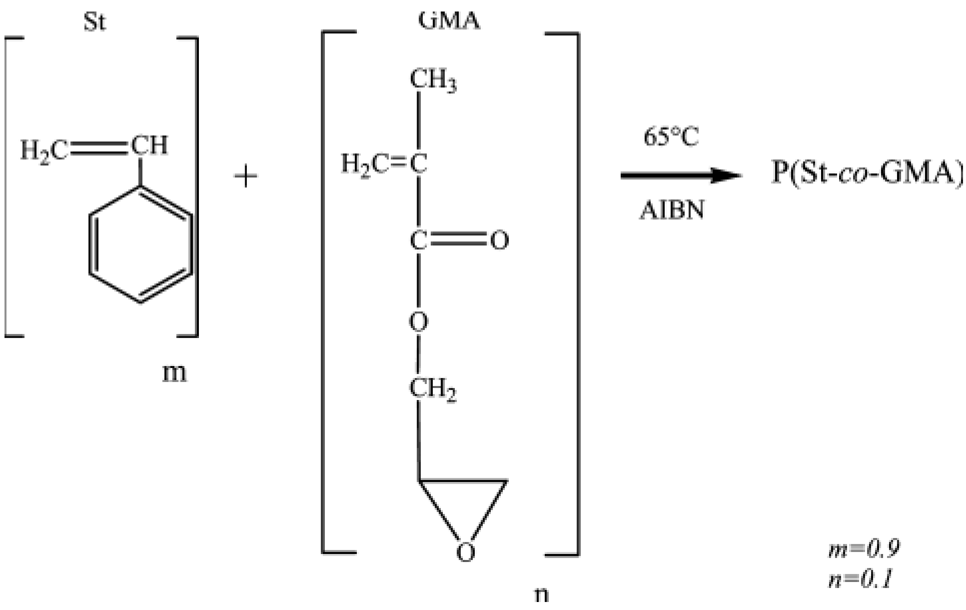

Figure 2.1: Schematic representation of Poly(Styrene-co-Glycidylmethacrylate) synthesis

2.2.2 Process Optimization for Electrospinning of Stimuli-Self-Crosslinkable P(St-co-GMA) nanofibers

An Optimization procedure was followed for desired fiber diameter and electrospinability time (see table 2.2). Firstly an optimization route was created for rendering the polymer concentration decision. For this purpose the ratio of crosslinking agent and the content of the GMA in the polymer kept constant, the initiator (TBA) and solution concentration were alternated.

Table 2.2: Process optimization route for Electrospinning of Self-Crosslinkable nanofibers

GMA content in polymer (% mol)	Initiator ratio (TBA/Polymer by weight)	Solution concentration (Polymer/DMF by weight)	Crosslinking agent ratio (PA/GMA functional group ratio)
%10	2%	10%	2
		15%	2
		20%	2
		30%	2
	4%	10%	2
		15%	2
		20%	2
		30%	2

Polymer solutions were prepared by dissolving P(St-co-GMA) 10, 15, 20, 30% (by weight) in DMF and stirring for 1 hour. After P(St-co-GMA) dissolved entirely 2 or 4% of catalyst tributylamine (TBA) and PA/Epoxide ring molar ratio (R) was kept constant for all samples as R: 2 and were added to copolymer solution and magnetically stirred for 30 minutes. An electrical bias potential (via Gamma high voltage ES 30P-20W) was applied to polymer solutions contained in 2 mL syringe, which has an alligator clip attached to the blunt stainless steel syringe needle (diameter 300 μm). The ground collector covered with aluminum foil and a syringe pump (NewEra NE-1000 Syringe Pump) was used. The applied voltage, solution flow rate and tip to ground distance were set at 15 kV, 0.4 ml/h, and 10 cm respectively during electrospinning. The polymer solution was electrospun onto the aluminum foil to obtain nonwoven fiber mats.

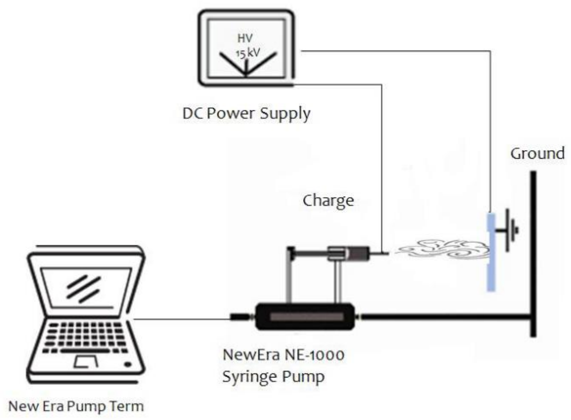

Figure 2.2: Illustration of electrospinning set-up

After solution concentration optimization was concluded. Optimized parameters kept constant and then calculated amounts of [PA/Epoxide ring molar ratio (R) is 0.5,1, 1.5, 2, 5, for 5 different samples] cross-linking agent Phthalic Anhydride (PA) were added to copolymer solution and the electrospinning procedure was repeated as mentioned above.

2.2.3 Crosslinking of Stimuli-Self-Crosslinkable P(St-co-GMA) nanofibers

The P(St-co-GMA) electrospun nanomats were cross-linked with post-heat-treatment by putting into an oven; the curing cycle was 2 hours at 90 ºC (just below polymer T_g to prevent morphological changes) and ramping 150 ºC with 2 ºC/min and keeping 1 hour at that temperature. The cross-linked fibers are called hereafter as P(St-co-GMA)/PA-TBA.

The proposed reaction route for P(St-co-GMA)/PA-TBA for the cross-linking is given in Figure 2.3. The reaction route for the epoxide and anhydride at presence of tertiary amine was described by Fischer[20]. Initiation of the reaction occurred by the activation of anhydride with tertiary amine to form carboxyl anion and carboxyl anion is reacted with the epoxide then generated an alkoxide anion to enable further reaction with the anhydride.

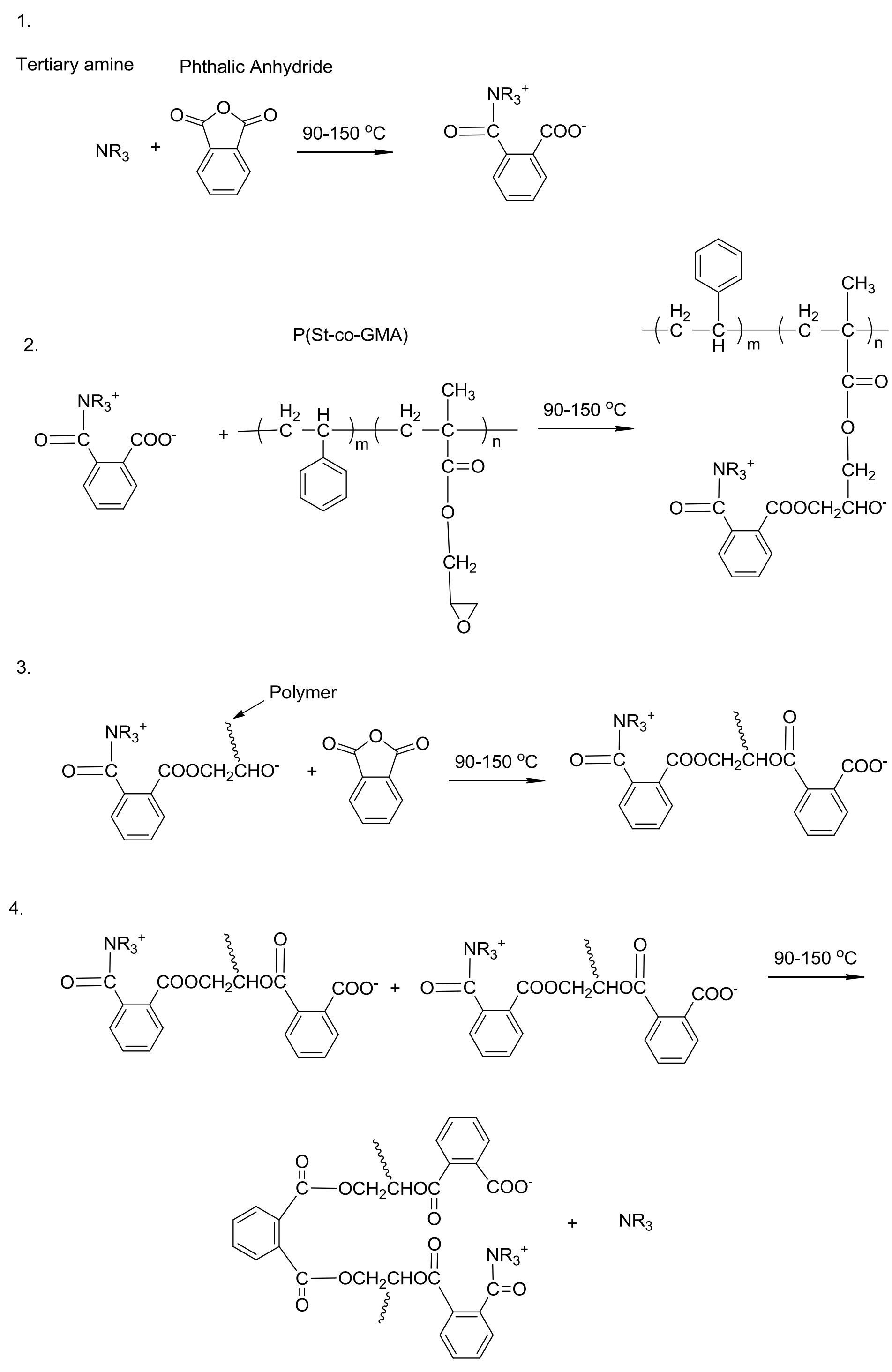

Figure 2.3: Proposed reaction route for crosslinking of P(St-co-GMA)/PA-TBA as-spun nanofibers.

2.2.4 Characterization of Electrospun Nanofibers

2.2.4.1 Solvent Resistance Measurement

The degree of cross-linking determination was performed by sol-gel analysis. P(St-co-GMA)/PA-TBA crosslinked fibers put in to an aggressive solvent (DMF) and kept soaked for 72 hours at room temperature. The swollen fibers were then cleaned with DMF and deionized water subsequently fibers were dried in a vacuum oven at 70 ºC. The experiments were performed with 5 pieces of the respective samples and then the extracted data were used as average in results and discussion section.

$$\%Sol\ Fraction = \left[\frac{(Mi-Mf)}{Mi}\right] * 100 \qquad (2.1)$$

$$\%Gel\ Fraction = 100 - \%Sol\ Fraction \qquad (2.2)$$

As a measure of cross-linking ratio gel fraction was calculated as in function 2.1 and 2.2 where Mi is the initial dry mass of sample and Mf is the dry mass of the extracted sample [1].

2.2.4.2 Spectroscopic Analysis

The structures of stimuli-self-crosslinkable and crosslinked P(St-co-GMA)/PA-TBA nanofibers were characterized by Attenuated Total Reflection Fourier Transform Infrared Spectroscopy (ATR-FTIR). Analyses were performed with Thermo Scientific iS10 FT-IR Spectrometer in the mid-infrared 4000 cm $^{-1}$ to 550 cm^{-1}.

2.2.4.3 Differential Scanning Calorimetry

The thermal properties of P(St-co-GMA), stimuli-self-cross-linkable P(St-co-GMA)/PA-GMA and cross-linked P(St-co-GMA)/PA-GMA nanofibers were characterized with Differential Scanning Calorimeter (Netzsch DSC 204). Thermal characterization of stimuli-self-crosslinkable nanofibers were done with a two dynamic cycle from 25 to 250 ºC. After then the glass transition (T_g) of previously crosslinked nanofibers were determined by means of one cycle dynamic scan from 25 to 250 ºC after crosslinking by cycle as mentioned before.

2.2.4.4 Morphologic Analysis

The morphologies of self-cross-linkable P(St-co-GMA) and cross-linked P(St-co-GMA)/PA-TBA electrospun mats was observed with a scanning electron microscope containing field emission gun (SEM LEO 1530VP) using secondary electron detector and in-lens detector at 2-5 kV after coating with Au-Pd for better electrical conduction. The diameter analyses of nanofibers were determined using ImageJ software analysis.

2.3 Results and Discussions

2.3.1 Electrospinability of Stimuli-Self-Crosslinkable P(St-co-GMA)/PA-TBA Nanofibers

Electro-spinning of initiator and crosslinking agent containing polymer solutions is demanding procedure to avoid premature cross-linking. The premature cross-linking may occur because of the temperature increase during magnetic stirring or effect of the high shear rate during electro-spinning. Therefore, we had initially focused on the electrospinability time of solutions. The collected data is given in Table 2.3. Consequently, the concentrated solutions and low concentrated also low viscous solutions were not able to be electrospun continuously. Additionally, the high initiator amount cause extreme viscosity changes and electrospinning were not achieved.

Finally, solution which had 15% solution concentration and 2% Initiator ratio (TBA/Polymer by weight) and 0,2% Crosslinking agent ratio (PA/GMA functional group ratio ‘R’) was chosen as ideal solution among the other trials therefore, further experiments were done with these optimized parameters.

Table 2.3: Electrospinability of different solutions

GMA content in polymer (% mol)	Initiator ratio (TBA/Polymer by weight)	Solution concentration (Polymer/DMF by weight)	Crosslinking agent ratio (PA/GMA functional group ratio 'R')	Nanofiber formation	Electrospinability time
%10	0,2%	10%	2	X	0
		15%	2	✓	>5 hours
		20%	2	✓	<1 hour
		30%	2	X	0
	0,4%	10%	2	X	0
		15%	2	X	0
		20%	2	X	0
		30%	2	X	0

2.3.2 Solvent Resistance of P(St-co-GMA)/PA-TBA Nanofibers

It is known that functional group (epoxide ring), polymer, cross-linker (PA) and catalyst (TBA) concentrations are the parameters for the cross-linking reaction [18, 23, 24]. We altered the PA to epoxide ring mole to mole ratio from 1:1 to 10:1 for five different stoichiometric ratios (R) while keeping the polymer and TBA concentrations constant.

The solvent resistance analyses showed that gel fraction of cross-linked fibers was between 95%-98.3% whereas P(St-co-GMA) nanomats were completely soluble in DMF solutions also again stimuli-self-crosslinkable P(St-co-GMA)/PA-TBA nanomats were entirely dissolved when putting into DMF solvent system before they were heat treated.

The cross-linking ratio of the P(St-co-GMA) nanomats is given in table 2.4. The weight loss is comparable, with an increasing amount of crosslinking agent ratio the crosslinking ratio increases till %98.3. Nevertheless among the five different crosslinking agent ratio there is not a significant gel fraction differences.

Table 2.4: Cross-linking ratio of P(St-co-GMA) nanomats among their crosslinking agent ratio (PA/GMA)

Crosslinking agent ratio (PA/GMA functional group ratio by mole fraction 'R')	Crosslinking ratio (% Gel Fraction)
R:0	0
R:1	95
R:2	97.7
R:5	98.2
R:10	98.3

Figure 2.4: Crosslinked P(Stco-GMA)/PA-TBA nanomats in DMF after 72 hours (R:2)

2.3.3 Spectroscopic Characterization of P(St-co-GMA) and P(St-co-GMA)/PA-TBA Nanofibers

FT-IR measurements performed prior to heat treatment and after the cross-linking to structurally verify the cross-linking of self-cross-linkable P(St-co-GMA)/PA-TBA nanofibers. Figure 2.5 shows the FT-IR spectra for P(St-co-GMA), self-cross-linkable and cross-linked P(St-co-GMA)/PA-TBA nanofibers. Each row includes self-cross-linkable and cross-linked nanofibers' spectrum pairs for an identical PA/Epoxide ring ratio. The characteristic bands of the reaction are at 1851 cm^{-1} and 1787 cm^{-1} [$\nu_{s,(C=O)}$ and $\nu_{as,(C=O)}$ of the anhydride ring], 902 cm^{-1} [$\nu_{s,(C-O)}$ overlapping epoxide (907 cm^{-1}) and anhydride (902 cm^{-1}) absorptions]. The intensities of the mentioned peaks decrease due to the reacting species during the cross-linking, aforesaid peak intensities also increases with the increasing PA/Epoxide ring ratio from 0.5 to 10 among the self-cross-linkable nanofibers. Also the characteristic epoxide ring stretching at 902 cm^{-1} becomes distinguishable after the cross-linking reaction due to the remaining oxirane ring moiety, these moieties decaying with the increasing PA/Epoxide ring ratio due to increasing extent of the cross-linking. Additionally intensity of the peak at 1727 cm^{-1} [$\nu_{s,(C=O)}$ ester] increases with the formation of the ester groups, which is also a proof of cross-linking[21, 25, 26].

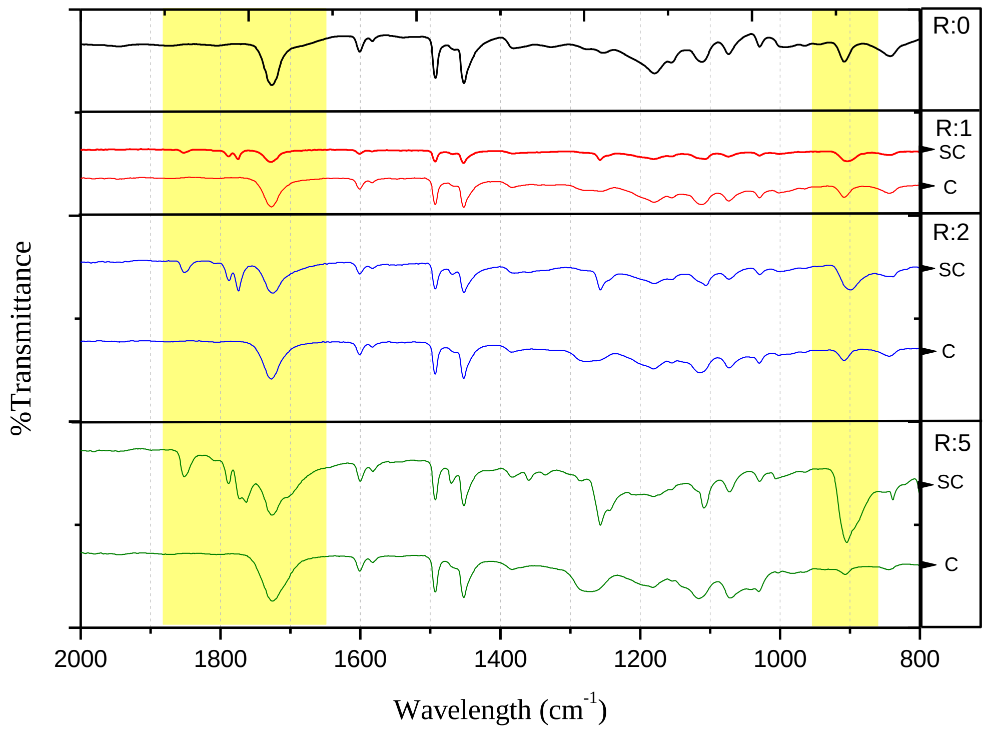

Figure 2.5: FT-IR spectrum of P(St-co-GMA) (R:0), self-crosslink-able (sc) and cross-linked (c) P(St-co-GMA)/PA-TBA nanofibers. Each row includes self-cross-linkable (above) and cross-linked (below) nanofibers' spectrum pairs for an identical PA/Epoxide ring ratio marked at the right column of the graph. Shaded areas involve characteristic bands of the system.

2.3.4 Differential Scanning Calorimetry of P(St-co-GMA) and P(St-co-GMA)/PA-TBA Nanofibers

Crosslinking is an exothermic reaction. For this reason to show heat treatment initiate the cross-linking process in our case a cure cycle were applied to untreated P(St-coGMA)/PA-TBA nanofibers. Figure 2.6 shows the reaction graphic for P(St-co-GMA)/PA-TBA nanofibers (R:2). The first heating cycle demonstrate that the exothermic reaction was acquired and the onset, peak and end temperatures are 65 ºC, 125 ºC, 150 ºC respectively. Sequentially the second heat cycle did show neither an exothermic reaction nor an endothermic reaction it only shows a glass transition temperature (T_g: 135 ºC). According to these characteristics the cross-linking reaction occurs exothermically, subsequent cycle shows after a heating cycle there is not an exothermic reaction pattern, therefore it can be said that the cross-linking reaction totally ended up.

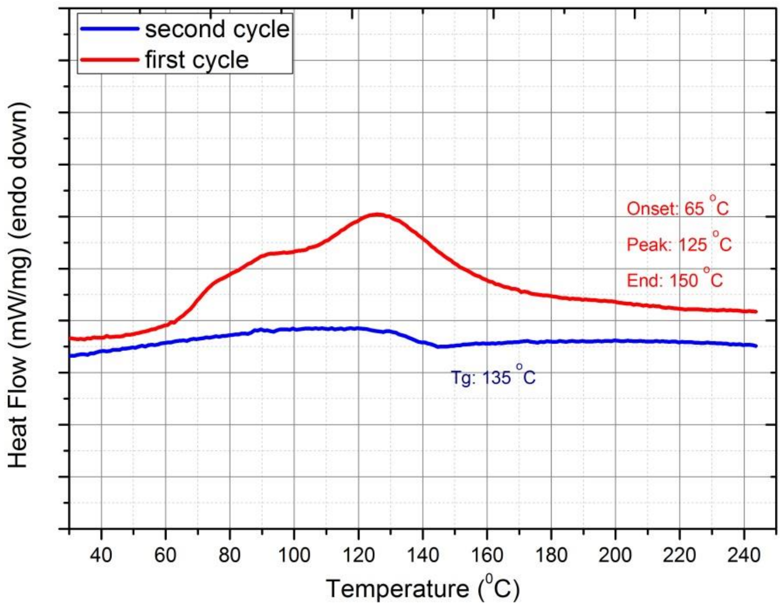

Figure2.6: The cure cycle of P(St-co-GMA)/PA-TBA nanofibers. (R:2) First heating cycle represented by red line and the second one shown by blue line. (Cross-linking Onset: 65 ºC, Peak: 125 ºC, End: 150 ºC)

DSC thermograms of cross-linked P(St-co-GMA)/PA-TBA and un-cross-linked P(St-co-GMA) nanofibers were carried out in order to identify the effects of the cross-linking on the thermal transitions of P(St-co-GMA) nanofibers (Figure 2.7). Self-crosslinkable P(St-co-GMA)/PA-TBA nanofibers were cured in an oven with a heating cycle which were not higher than the glass transition temperature of un-crosslinked P(St-co-GMA) nanofibers.

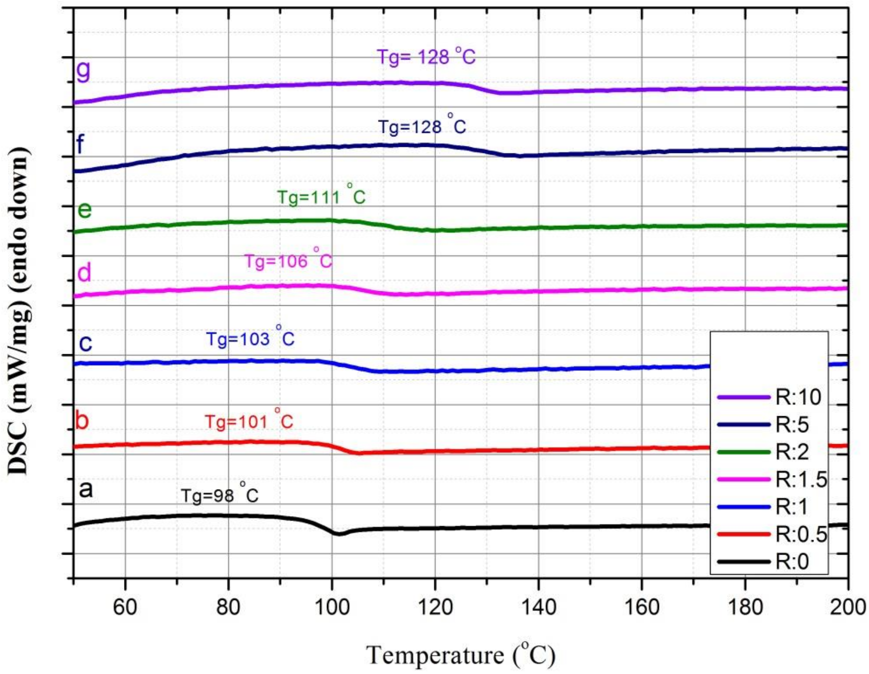

Figure 2.7: DSC curves of uncross-linked P(St-co-GMA) (a, R:0) and crosslinked(b-g) P(St-co-GMA)/PA-TBA nanofibers. PA to epoxide ring ratio (R) for b-g 0.5, 1, 1.5, 2, 5, 10 respectively.

Glass transition temperature of nanofibers enhance from 98 ºC (P(St-co-GMA)) to 128 ºC with the increasing PA/ Epoxide ring ratio up to 5 due to decreasing flexibility of polymer chains with the increasing extent of the cross-linking. After that point further increment of the cross-linker does not increase the glass transition temperature since the cross-linking ratio does not get higher with addition of extra PA.

Additionally, the difference between the glass transition temperatures of nanofibers which were cured in DSC and in an oven should be discussed. The reaction medium for the DSC case was inert and very stable but in oven conditions the reaction occurred in air medium and was not stable as DSC. The inertness and stability could possibly cause a superior ability to reaction due to enhanced network, and consequently glass transition temperature of DSC cured nanofibers is higher.

2.3.5 Morphplogical characterisation of P(St-co-GMA) and P(St-co-GMA)/PA-TBA Nanofibers

Fiber morphologies of P(St-co-GMA), self-cross-linkable and cross-linked nanofibers are examined for the selected PA/Epoxide ring ratios. The morphologies of nanofibers prior to heat treatment, after heat treatment 90 ºC (below the T_g of the fibers) for 2h and post heat treatment at 150 ºC (above the T_g of the fibers) for 1 hour shown with the additional fiber diameter distribution charts in figure 2.7. Morphological analyses confirm that the fibrous morphology is obtained for the selected electrospinning parameters. Additionally SEM images of the nanofibers prior to heat treatment demonstrate that bead free, randomly oriented continuous fiber formation was achieved. After the heat treatment at 90 ºC fiber morphology remained intact however shrinkage observed it can be ascribed to the conformational changes of the polymer chains and/or to release of the solvent molecules during heat treatment[16]. Further heat treatment at 150ºC cause morphological changes for uncross-linked and cross-linked fibers because the temperature higher than the glass transition temperature of nanofibers.P(St-co-GMA) nanofibers which are uncross-linked could not maintain their fibrous structure over their T_g (see Figure 2.7 c). Above the T_g of the fiber webs the softening effect on the webs cause individual interaction between the fibers and cause to lose fibrous structure. Cross-linked fibers maintained their fibrous structure but for the cases $R \leq 2$ fibers transformed from circular thin fibers to ribbon-like thicker flattened fibers (see Figure 2.7 l) and the level of the transformation decreases with the increasing amount of PA due to the increasing cross-linking ratio also T_g of the nanofibers. This phenomenon can be ascribed to chain mobility over the T_g of the cross-linked network. Formed cross-linked network could not restrict the softening of the fibers. Furthermore, above the T_g of the fiber webs the softening effect on the webs cause individual interaction between the fibers and cause to lose fibrous structure. Additionally, average fiber diameters of nanofibers are given in the Table 2.5.

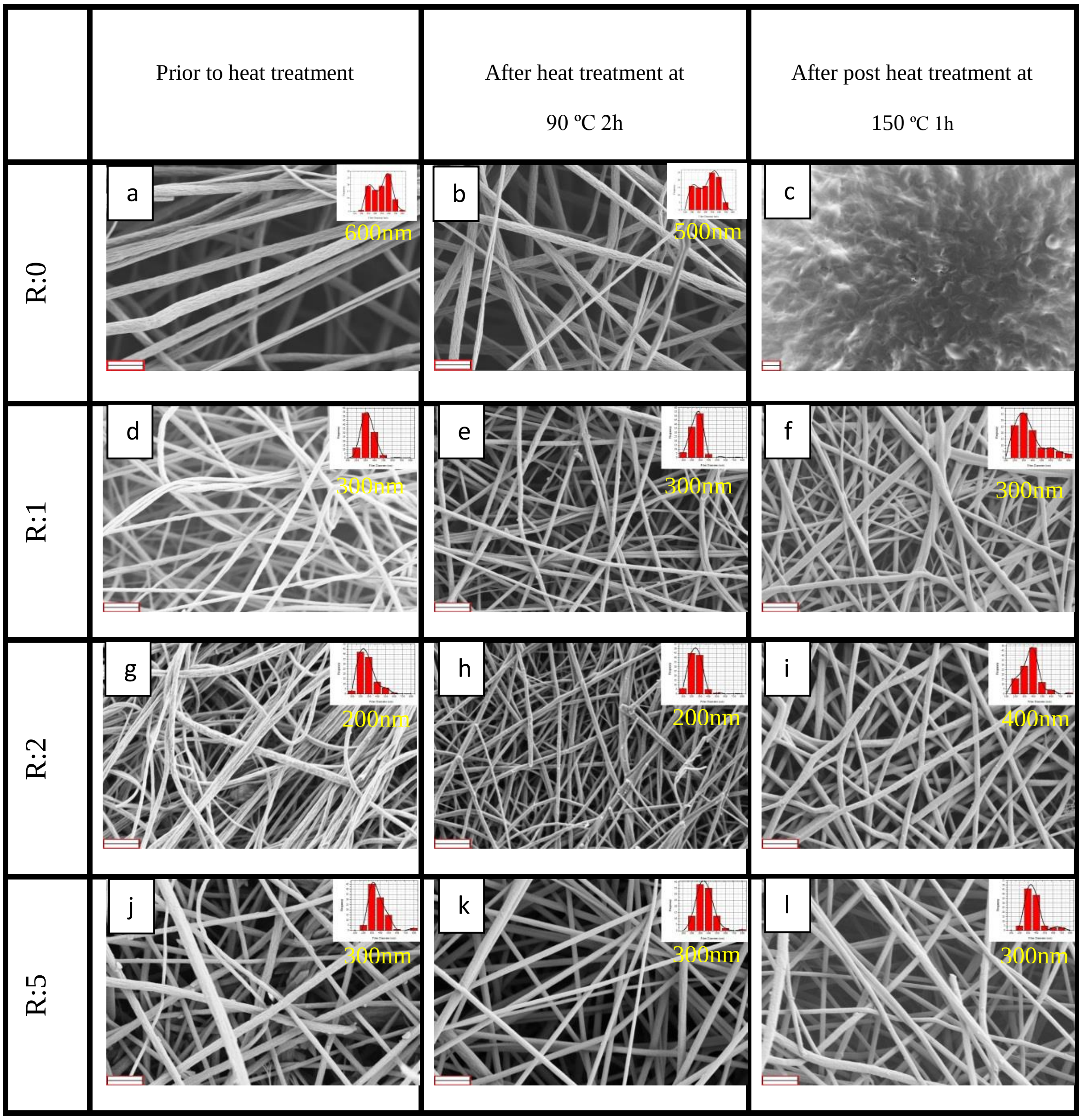

Figure 2.8: SEM micrographs of electrospun fibers. Each row includes SEM images of the fibers with an identical PA/Epoxide ring ratio. Each raw includes SEM images of the fibers prior to heat treatment (left), after heat treatment at 90 ºC 2h (center), post heat treatment at 150 ºC (right). (for a,b,d-l scale bar: 2µm and for c scale bar: 20µm) (Nanofiber diameter distribution chart present fiber diameters from 100 to 800nm and each column represent a hundred nm range also distribution graphs include the highest bar’s scale below)

Table 2.5: Average fiber diameter distributions

Crosslinking agent ratio (PA/GMA functional group ratio by mole fraction 'R')	Average Fiber Diameter (nm) - Standard deviation		
	Pre-heat treatment	**After heat treatment (90 ºC 2 hours)**	**After Post-heat treatment (150 ºC 1 hours)**
R:0	455 - 140	394 - 141	Fibrous form was not observed
R:1	271 - 64	207 - 63	317 - 150
R:2	233 - 87	199 - 66	309 - 103
R:5	318 - 100	308- 97	308 - 93

The purpose of the cross-linking study was to produce thermally stable P(St-co-GMA) nanofibers. For this reason to enable to show the stability differences of cross-linked and un-cross-linked P(St-co-GMA) nanofibers, an unprecedented way of electrospinning was applied via electrospinning P(St-co-GMA) and P(St-co-GMA)/PA-TBA solutions onto same collector with different pumps (dual syringe technique). Then curing cycle was applied to collected nanomats then morphological analysis was done for each step of the curing (See figure 2.8).

PA/GMA	**Pre-heat treatment**	**After heat treatment (90 ºC 2 hours)**	**After Post-heat treatment (150 ºC 1 hours)**
R:0 and R:5	a 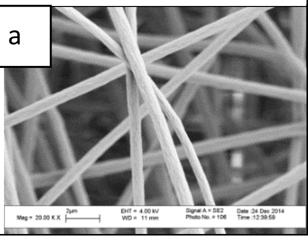	b 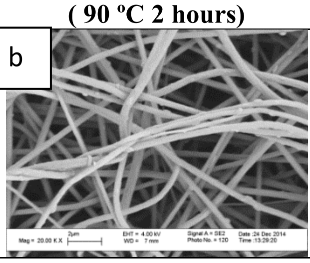	c 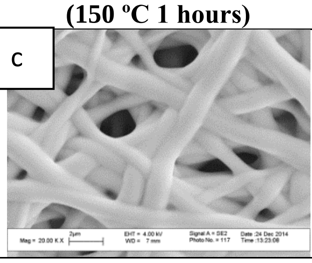

Figure2.9: SEM micrographs of P(St-co-GMA) and P(St-co-GMA)/PA-TBA nanofibers' prepared by dual syringe technique

SEM micrographs of the mixed nanofibers demonstrate that the un-crosslinkable P(St-co-GMA) nanofibers could stand till their glass transition temperature (figure 2.9 b) however higher temperatures cause melting of the P(St-co-GMA) nanofibers. Figure 2.9 c demonstrates that melted nanofibers covered the cross-linked P(St-co-GMA)/PA-GMA nanofibers' surface.

Mag.	PA/GMA Ratio	
	R:1	R:5
5K	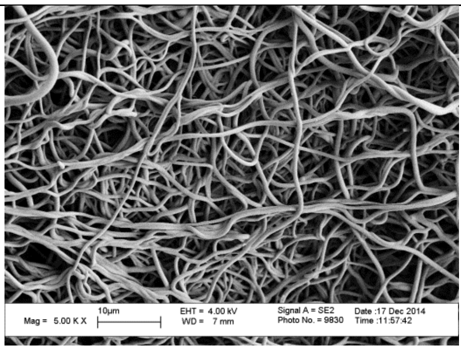	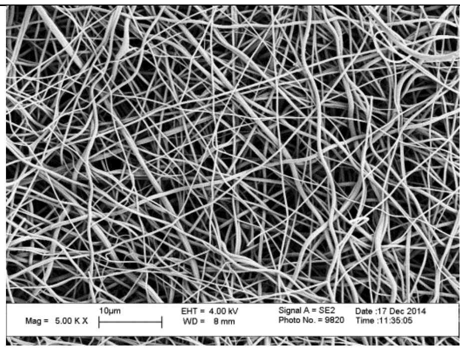
10K	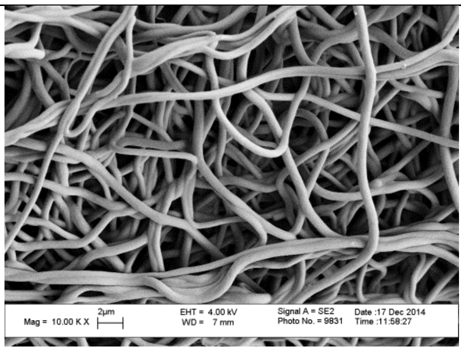	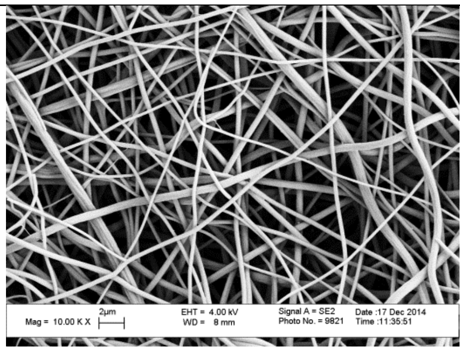
20K	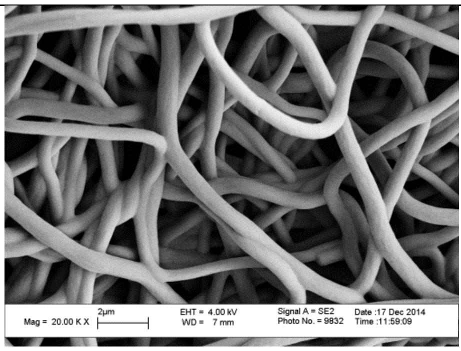	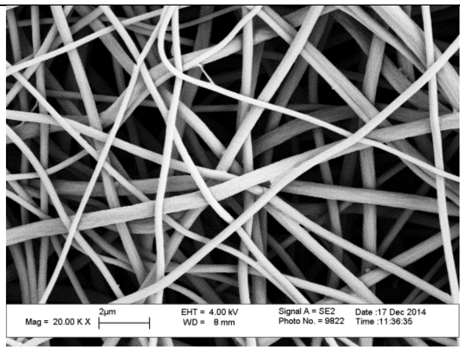

Figure 2.10: SEM micrographs of P(St-co-GMA)/PA-TBA nanofibers with PA/GMA ratios R:1 and R:5 after immersion in DMF 72 h. (For neat samples please see figure 2.8)

Table 2.6: Average fiber diameter distributions before and after the swelling tests

PA/GMA	**Average Fiber Diameter (nm) - Standard deviation**	
	Before Swelling test	After Swelling test
R:1	271 - 64,20	648,36 -118,96
R:5	318,29 - 100,49	340,40 – 103,95

Figure 2.10 shows the SEM photos of the crosslinked P(St-co-GMA)/PA-TBA nanofibers with PA/GMA mole ratio R:1 and R:5 after immersion in organic DMF solvent for 72 h at room conditions. Comparison with the neat P(St-co-GMA) nanofibers which are available in figure 2.8 d (R:1) and j(R:5). It can be seen that the crosslinked nanofibers, which are with a PA/GMA ratio R:5, are rather unaffected although the P(St-co-GMA) nanofibers have an aggressive solubility in DMF solvent. The average fiber diameter analysis was done after the swelling tests (Table 2.6). The average fiber diameter increased 140% for the R:1 case however for the R:5 case the swelling of the fiber diameter' were only 6%. It should be noted that crosslinked PANGMA copolymers which are crosslinked by immersion to crosslinking agent studied by Dai et al[11]. Dai also investigated the morphologies of crosslinked PANGMA nanofibers after swelling in DMF solvent and reported as DMF cause ribbon-like swelling with surface erosion. However our results shows that the harsh environment of the DMF solvent has not affected the P(St-co-GMA)/PA-TBA nanofibers. Consequently the crosslinked P(St-co-GMA)/PA-TBA nanofibers have superior solvent resistance and therefore are very suitable for the applications in aggressive solvent environments.

2.4 Concluding Remarks

In order to introduce stimuli-self-crosslinking ability to P(St-co-GMA) nanofibers a chemical route was established by the addition of different ratios of crosslinking agent PA and initiator TBA to the system. Electrospinning parameters were optimized to enable time independent stimuli-self-crosslinkable nanofibers without rheological constraints. As a result of thermal characterizations an increase of 30 ºC in glass transition temperature was obtained. FT-IR analysis confirmed the chemical reaction between the epoxide group of GMA and anhydride groups of PA by the initiation of catalyst TBA. FT-IR analysis was supported with the swelling measurements and 98.3% crosslinking ratio was acquired. Finally microscopic determination was done before and after thermal process applied and morphological changes was not detected.

CHAPTER 3

DEMONSTRATION ON COMPOSITES

STRUCTURAL COMPOSITES HYBRIDIZED WITH EPOXY COMPATIBLE IN-SITU CROSS-LINKED POLYMER NANOFIBROUS INTERLAYERS

3.1 Introduction

Polymer based nanofibers manufactured by electro-spinning are strong candidates for interlaminar toughening of composite laminates. They can enhance mechanical performance significantly in most of the composite applications without considerable weight increase. Numerous studies in the literature [27],[28] present efforts to show their potential. Recent works of our group,[1], [3], [6], [8] also highlight incorporation of the nanofibers as the interlayers and associated delamination and transverse matrix-cracking resistance of nano-interlayered laminates both through out of plane and in-plane testing. The concept of toughening with nanofibrous interlayers begins with designing/selecting a base polymer (see Table 3.1 for the variety of polymers introduced as interlayers). The suitable choice of the nanofibers is the initial, but the vital part for the successful practice. The relevant key factors to mark are solubility of the polymer, and its electrospinnability in the form of fibers. Problem free electrospinning of a polymer solution is typically expected to provide uniform fiber spinning without bead formation. Compatibility with the matrix/resin of composite material and resin curing conditions is also decisive. It is of paramount importance that the nanofiber material should facilitate strong chemical bonding and interface compatibility. Moreover thermal stability of the interlayer fibrous morphololgy (such as above glass transition and melting temperature) is arguably essential and should be in compliance with the curing cycle of matrix system as the distortions on the morphology may affect the failure mechanisms and mechanical behavior. It is worth to underline the temperature dependent behavior because typical high performance composite applications are of high temperature cure systems. In the light of this issue, current work firstly shows the effect of above T_g exposure on the nanofibrous interlayer morphologies such as the curing temperature of carbon/epoxy prepreg system. Secondly, it offers a unique in-situ crosslinking methodology where crosslinking of nanofibers takes place during the consolidation of composite laminates before the T_g of nanofibers is exceeded. Lastly, it shows the mechanical performance differences for un-crosslinked nanofiber interlayered laminates and heat stimuli-self-crosslinked nanofiber interlayered laminates when they both are cured above Tg of the nanofibers. The hypothesis is that stimuli-self-crosslinking enables a homogenous crosslinking regime for the nanofibers while epoxy matrix is cured as such better mechanical performance can be achieved. This methodology is applicable and usable for nearly all acrylic and dominantly amorphous engineering polymers. An example case is demonstrated where stimuli-self-crosslinked P(St-co-GMA) nanofibers are added as interlayers to carbon/epoxy prepreg composites for which the curing cycle demands 150°C or higher. Interlayered laminates are subjected to three-point bending and mode II shear tests. Mechanical test outputs are supported with cross-sectional and fracture surface microscopy analysis through Scanning Electron Microscopy.

Table 3.1: Literature review for nanofiber interlayered studies

Author/Year	Polymer matrix/prepreg	Nano reinforcement/ nanofiber material	Experiment/ Test	Highlighted investigation/results
J.S.Kim et al[27]/ 1999	Epoxy	Polybenzimidazol	3-Point Bending Double Torsion	Elastic modulus % 27 K_{IC} % 63 G_{IC} % 263
	Rubber		Tension Tear	Elastic modulus % 988 Tensile Strength % 33 Tear Strength %91
Dzenis et al[29] / 2009	Carbon/ epoxy	Polybenzimidazol	DCB	G_{IC} % 15
			ENF	G_{IIC} % 130
S.Sihn et al [30]/ 2008	Carbon/ Epoxy	Polycarbonate	Tension	Micro crack initiation % 8.4 , delamination % 8.1
L.Liu et al [31]/ 2006	Glass fiber/ Epoxy	PA6	Tension 3-Point Bending	Epoxy 609 < PA6 < TPU Tensile Strength. Epoxy 609 > PA6 > TPU Tensile modulus
		Epoxy 609		
		TPU		
L.Liu et al [32]/ 2008	Glass fiber/ Epoxy	Epoxy 609	ENF	G_{IIC} % 9
S.H.Lee et al [33]/2008	Carbon fiber/ Epoxy	Non-woven carbon fabric	ENF DCB	G_{IIC} % 259 G_{IC} % 28
S.H.Lee et al [34]/2002	Carbon fiber/ Epoxy	Non-woven carbon fabric	ENF	G_{IIC} % 260
R. Palazzetti et al[35]/ 2011	Epoxy/ Carbon fiber(0/90)	Naylon 6,6 nanofiber mat	DCB ENF	G_{IC} %5 Absorbed Energy %23 Absorbed Energy %8.1 Maximum stress 6.5
Elif Özden et al [1]/ 2010	Epoxy	P(St-co-GMA) /EDA	3-Point Bending	Flexural modulus % 30 Flexural Strength %23
		P(St-co-GMA)		Flexural modulus % 27 Flexural Strength %16
		PSt		Flexural modulus % 27 Flexural Strength %16
Kevin Magniez et al[36]/ 2011	Epoxy/ Carbon fiber	poly(hydroxyether (bisphenol A)) (phenoksi)	DCB ENF	G_{IC} %118 G_{IIC} %30

J. Zhang et al[37]/2010	Epoxy/ Carbon fiber	Polyetherketon cardo	DCB	G_{IC-INI} %60 $G_{IC-PROP}$ %81
J. Zhang et al[38]/2012	Epoxy/ Carbon fiber	poly(e-caprolactone)	DCB	G_{IC-INI} %37 $G_{IC-PROP}$ %92
Daniel R. Bortz et al[39]/ 2011	Epoxy/ Carbon fiber ±45	Helical Carbon nanofiber	DCB	G_{IC} %35
Masahiro Arai et al [40]/2012	Epoxy/ Carbon fiber	VGCF, VGCF-S, MWNT-7	DCB ENF Mixed mode Flexural	G_{IC} 2.3 fold G_{IIC} 3.6 fold
Kaan Bilge et al[6]/ 2012	Epoxy/ Carbon fiber	P(St-co-GMA)	ENF	G_{IIC} % 55
			Un-notched Impact	Absorbed Energy % 8
			Transversial Tension	Transversal Tensile Strength % 17
		P(St-co-GMA) /MWCNT	ENF	G_{IIC} % 70
			Un-notched Impact	Absorbed Energy % 20
			Transversial Tension	Transversal Tensile Strength % 27
Daniel R. Bortz et al[41]/ 2011	Epoxy (amine cured)	Helical Carbon nanofiber	3-Point Bending	G_{IC} %144 K_{IC} %78
			Tension-Tension Fatigue	Fatigue Life %365
S. Zainuddin et al[42]/ 2010	Glass fiber/ Polyurethane/ epoxy sandwich composite	Carbon nanofiber (dispersed in polyurethane foam)	Semi-static creep	Creep Strength 33% Creep modulus 19%
			Creep Fatigue Test	400000 cycle
Christopher S Grimmer et al[43]/2008	Glass fiber/ Epoxy	Carbon nanotube	Tension-Tension Fatigue	Long cycle fatigue resistance 60% -250%
Yuanxin Zhou et al[44]/ 2008	Epoxy/ Carbon fiber (VDRTK)	Carbon nanofiber	Tension-Tension Fatigue	Increase in Fatigue life
			3-Point Bending	Flexural Strength %22.3
			Tension	Tensile Strength %11
C. M.Manjunatha et al [45]/2010	Glass fiber/ Epoxy	Micro rubber particles (CTBN)	Tension Fatigue Test	Fatigue Life inc. 3 fold
C. M.Manjunatha et al[46]/2010	Glass fiber/ Epoxy	CTBN and Silica nano particles	Tension Fatigue Test	Fatigue Life inc. 6-10 fold
C. M. Manjunathav et al [47]/ 2010	Glass fiber/ Epoxy	Silica nano particles	Tension Fatigue Test	Fatigue Life inc. 3-4 fold
Mohammad A. Rafiee et al[48]/ 2010	Epoxy	Grafene	Tension Fatigue Test	Crack Propagation slowdown 25 fold

3.2 Experimental Procedure

3.2.1 Electro-spinning and Laminate Manufacturing

Self-Crosslinkable polymeric nanofibers were produced via electrospinning. The production parameters were electrical bias, flow rate and tip to collector distance which were set at 15 kV, 0.5 mL/h, 15 cm respectively (see figure 3.1). Pre-cut carbon/epoxy prepreg layers were supplied by AKSA Akrilik Kimya San. A.Ş. which were placed over the grounded collector. Then the polymer solution was electrospun directly onto the prepreg surface. Despite depositon weight penalty due to the homogenously applied nanofibrous interlayer is negligible, each as low as 0.2% of the hosting prepreg ply weight.

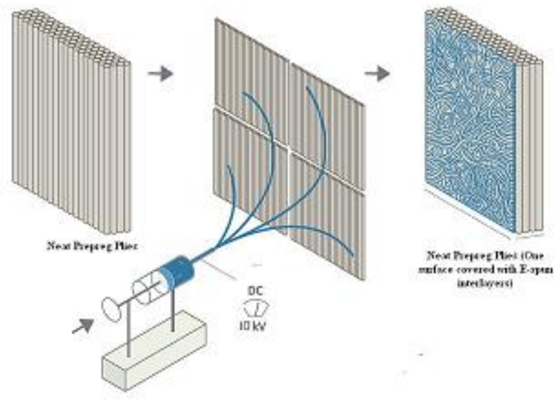

Figure 3.1: Illustration of the electro-spinning over the prepreg plies

Note that, out-of-the freezer time and conditions of the prepared plies were kept consistent throughout the study, whether being subject to electrospining (for reference specimens and testing) or not. 3-point bending tests were done on composites produced from the prepreg with ply thicknesses of 0.267 mm, whereas ENF tests were done on composites produced from a prepreg of 0,067 mm nominal cured ply thickness. After stacking the plies for intended laminates, each stack was put on a metallic mold along with a release film and peel ply (see figure 3.2). Over the pile of plies another peel ply sheet and breather layer were applied (see figure 3.3). Finally the whole lay-up was vacuum bagged and kept under vacuum during the consolidation. The cure cycle was selected primarily in accordance with the crosslinking temperature and glass transition of the self-crosslink-able P(St-co-GMA)/PA-TBA nanofibers (as explained in Chapter 2) therefore, cure cycle was set as 2 hours at 90 ºC (lower than the T_g of P(St-co-GMA) nanofibers) later 2 additional hours at 135 ºC. However P(St-co-GMA) nanofiber interlayered structural composites cured with cycle 1 (see table 3.2)

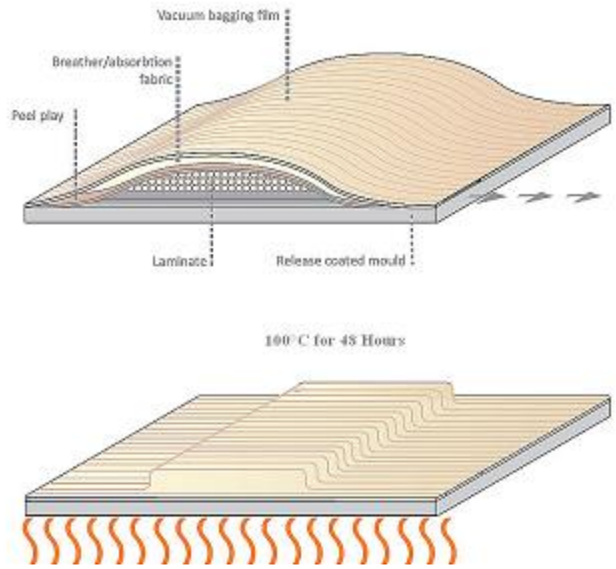

Figure 3.2: Vacuum Bagging and Curing Process

Table 3.2: Cure cycles that subjected to structural composites

	Heating Rate (ºC/min)	Intermediate Step (ºC)	Curing Temperature (ºC)	Polymer Type	T_g
Cycle 1	10	-	100	P(St-co-GMA)	100
Cycle 2	10	90	135	P(St-co-GMA)	100
				P(St-co-GMA)/PA-TBA	128

3.2.2 Mechanical Testing

Zwick Roell Z100 Universal Testing Machine was used for mechanical testing. Loading rates and machine accessories were set up in accordance with the testing types and associated test standards.

3.2.2.1 3-Point Bending Tests

Flexural strength and modulus of (0/0/0) laminates were evaluated via three point bending tests. Interlayered laminates were produced by deposition of interlayer onto individual carbon/epoxy prepreg plies. Specimen preparation and testing conditions were determined according to ASTM D790 standard. Applied load versus crosshead displacement values were recorded and corresponding flexural strength ($\boldsymbol{\sigma_f}$) and flexural modulus ($\mathbf{E_B}$) values were calculated as follows:

$$\boldsymbol{\sigma}\mathbf{f} = \frac{\mathrm{PL}}{2\mathrm{bd}^2}$$

$$\mathbf{E}_{\boldsymbol{B}} = \mathrm{L}^3 \frac{m}{4bd^3}$$

where P is the maximum load, m is the slope of the tangent to the initial straight-line portion of the load displacement curve and b, d, L are specimen width, thickness and span length respectively.

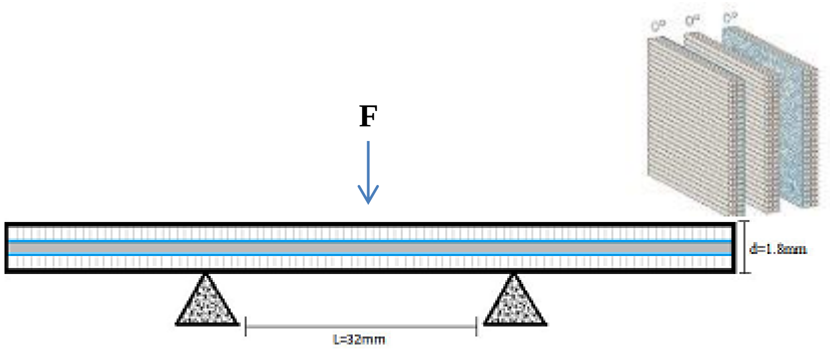

Figure 3.3: Three-point bending test configurations and lamination sequences

3.2.2.2 End Notched Flexure (ENF) Test

Mode II critical strain energy release rate (G_{IIC}) of the laminated composite structures was determined by ENF test results. $(0)_{48}$ uni-directional (UD) laminates containing delamination at the mid-surface were tested under 3-point bending load configuration according to ASTM D7905 (Standard Test Method for Determination of the Mode II Interlaminar Fracture Toughness of Unidirectional Fiber-Reinforced Polymer Matrix Composites). During the preparation of the laminates a non-adherent 30 μm thick film layer was placed to create the initial delamination for ENF testing additionally electrospun nanofiber interlayer was applied only at the mid plane. Tests were conducted with a constant displacement rate of 1mm/min and G_{IIC} values were calculated using direct beam theory [49].

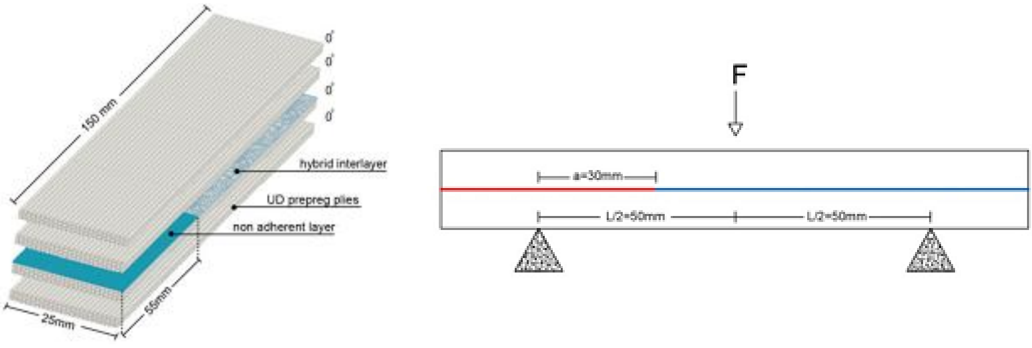

Figure 3.4: ENF test configuration

3.2.3 Surface and Cross Sectional Characterization

Fracture surface and cross sectional analysis of the tested laminated composites were carried out with a scanning electron microscope containing field emission gun (SEM LEO 1530VP) using secondary electron detector at 2-5 kV after coating with Au-Pd for better electrical conduction.

3.3 Results and Discussion

3.3.1 Optimization of Reinforcing Nanofibrous Layer Amount

The first step of mechanical characterization efforts was to investigate if the areal density of electrospun nanofibrous interlayers (or thickness) was effective in the flexural performance of the composite laminates. In order to do this, we have used our conventional P(St-co-GMA) nanofibers without any crosslinking agent addition. The composite laminates were cured according to curing receipt 1 (see table 3.2-cycle 1). The interlayer depositon amount is varied by the polymer solution volume for a given collector area. That is, the variable can also be introduced as areal density, gram per square meter (GSM). GSM value calculated by the equation which is given below where V is solution volume (ml) C is solution concentration (g polymer/ solution volume) and A is electrospinning area (m^2),

$$GSM = \frac{V * C}{A}$$

The electrospinning conditions were set as the same for all cases. With an increase in the electrospinning solution volume from 0.25 to 1.5 ml, electrospinning was done directly onto the 15×15 cm^2 prepreg plies. Fabricated laminates have $(0)_3$ stacking sequence. Finally 3-point bending tests were done to investigate flexural properties of laminates as a function of interlayer areal density (or thickness).

Table 3.3: 3-Point Bending test results for optimization

Polymer Solution Amount	ml Volume	Neat	0,25	0,313	0,375	0,438	0,5	0,75	1,5
	g/m^2 GSM Calculated	Neat	4,4	5,6	6,7	7,8	8,9	13,3	26,6
Flexural Strength (MPa)		1255	1312	1371	1454	1404	1351	1251	1168

Figure 3.6 shows that the increasing amount of interleaving reinforcement increased the flexural strength to maximum point where GSM was 6,7 corresponding to polymer solution volume of 0,375 ml. Further increase of nanofibrous layer areal density led to decrease on flexural strength although it was higher than the non-interleaved strength upto a critical value. Beyond this critical limit, interlayer degraded the flexural response that is attributed to the degradation of the effective adhesion between the plies. These results indicate that there is an optimum for the best of interlayers. Although interfacial compatibility between P(St-co-GMA) based polymeric nanofibers and the epoxy resin is in effect [1, 3, 6-8], excessive use of them may result in the mechanical performance of the laminates to deteriorate due to adverse effects on interaction level in the inter-ply adhesion zone [37].

As a consequence the decision was reached to use the amount of 6,7 GSM (0,375 ml) for further mechanical experiments.

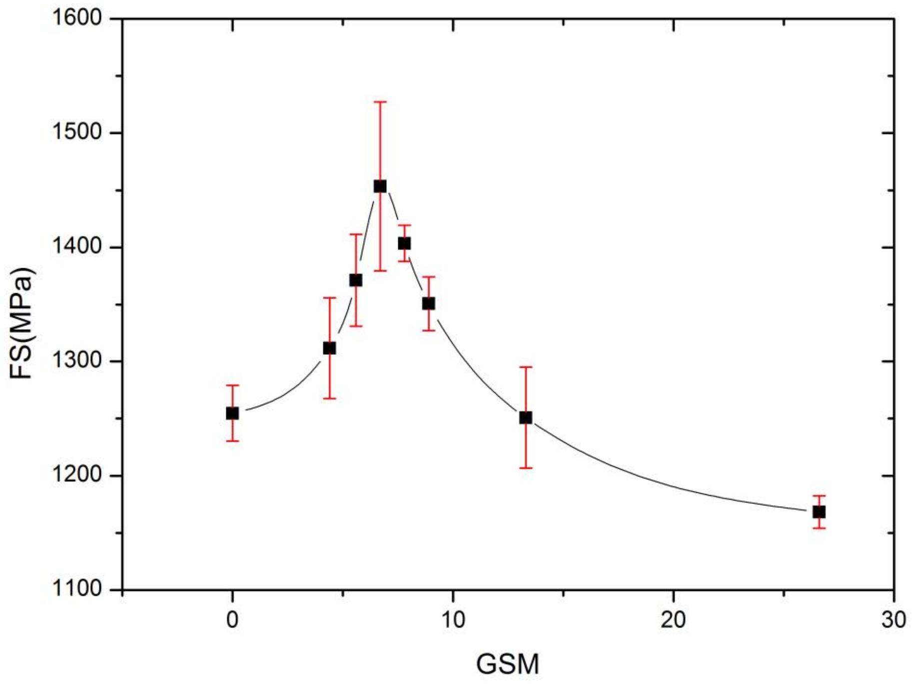

Figure 3.5: Influence of reinforcement amount on flexural properties

3.3.2 Structural Compatibility of Stimuli-Self-Crosslinkable P(St-co-GMA)/PA-TBA interlayers and Epoxy

Figure 3.6 show the SEM images of P(St-co-GMA) and stimuli-self-crosslinkable P(St-co-GMA)/PA-TBA nanofibers electrospun onto the prepreg surfaces after heating to 135 ºC. The magnified images show clearly the nanofibers' morphologic changes by the influence of high curing temperature and interaction with the epoxy.

Mag.	P(St-co-GMA) Nanofibers onto prepreg surfaces	Stimuli-Self-Crosslinkable Nanofiber onto prepreg surfaces
500	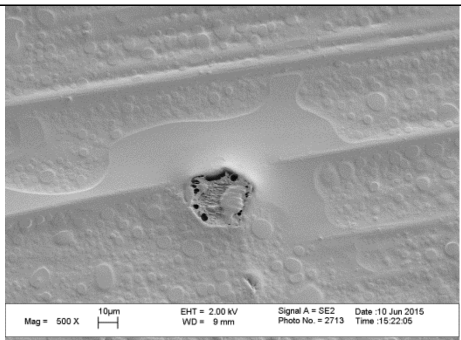	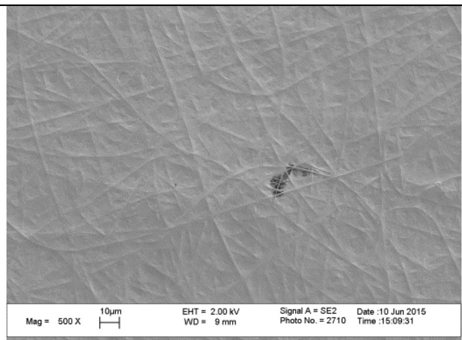
1K	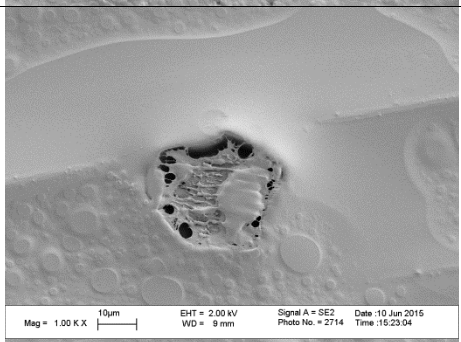	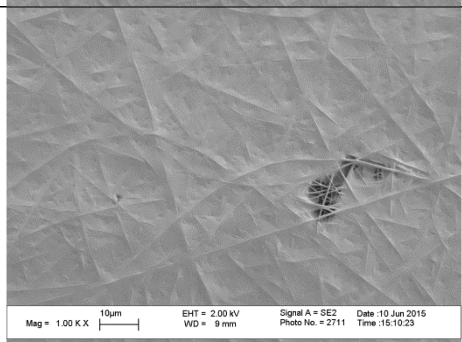
5K	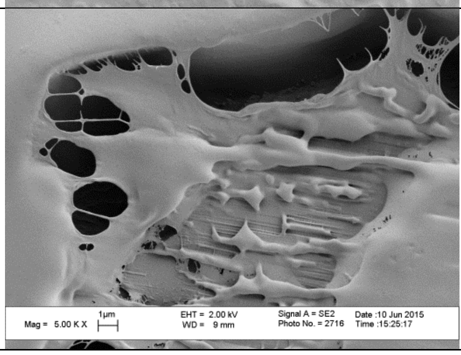	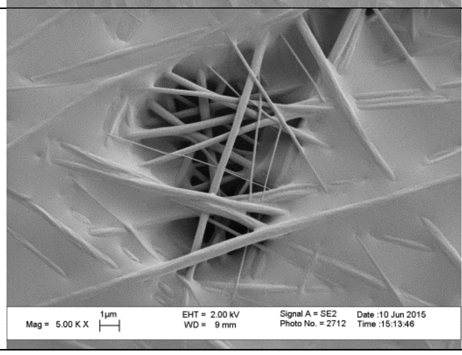

Figure 3.6: P(St-co-GMA) (left) and Stimuli-Self-Crosslinkable (right) Nanofibers onto prepreg surfaces cured at 135 ºC (Magnifications: 500, 1K, 5K)

The left side SEM images at the figure 3.6 which belong to P(St-co-GMA) nanofibers seem bead like polymeric islands transformed from the fibrous network. When the image is further magnified over the epoxy poor region it is clear that fibrous form/network changed and nanofibers are no longer distinctly exist,. However at the right side of the figure 3.6 Stimuli-Self-Crosslinkable P(St-co-GMA)/PA-TBA nanofibers can be seen and it is evident that fibrous form and their integrity were not influenced by above Tg heating scheme. It is important to confirm that epoxy and the stimuli-self-crosslinkable nanofibers are also structurally compatible (see the magnified images). Randomly oriented nanofibers at the surface of the prepreg plies can easily be seen despite being after above Tg heat treatment.

Nanofibrous mat over the prepreg layers After the electrospinning	Nanofibrous mat over the prepreg layers After curing at the 135 ºC
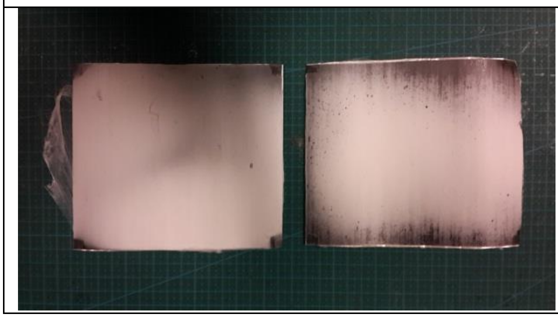	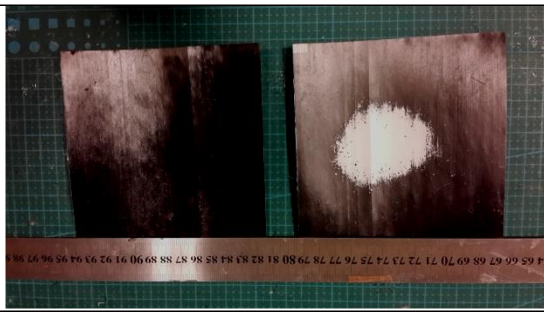

Figure 3.7: Nanofibrous mat over prepreg layers (P(St-co-GMA) nanofibers at left, Stimuli-self-crosslinkable P(St-co-GMA)/PA-TBA nanofibers at right)

To macroscopically investigate that interaction with nanofibrous layers and epoxy prepreg surfaces at the center of the prepreg plies a nanofiber rich area was deliberately created to prevent the completely wetting of the fibers at that area (Figure 3.7). Consequently excessive amount of stimuli-self-crosslinkable nanofibers at the center could not get wet completely and also maintain the fibrous form. This is also a brute force representation of the effect of excessively thick nanofibrous interlayer mentioned in the previous section. However the P(St-co-GMA) nanofibers were transformed into a polymeric coat at the surface of the prepreg, which apparently wetted thoroughly by the epoxy.

3.3.3 Flexural Performance by 3-Point-Bending Tests

Results of 3-point bending tests of laminates interlayered with stimuli-self-crosslinkable P(St-co-GMA), P(St-co-GMA) nanofibrous mats and also not interlayered reference neat composite laminates, suggest that the addition of the P(St-co-GMA) cause decrement in flexural properties, however introducing stimuli self-crosslinkable P(St-co-GMA) nanofibers let to increase in both flexural strength and modulus of the samples at high curing temperatures.

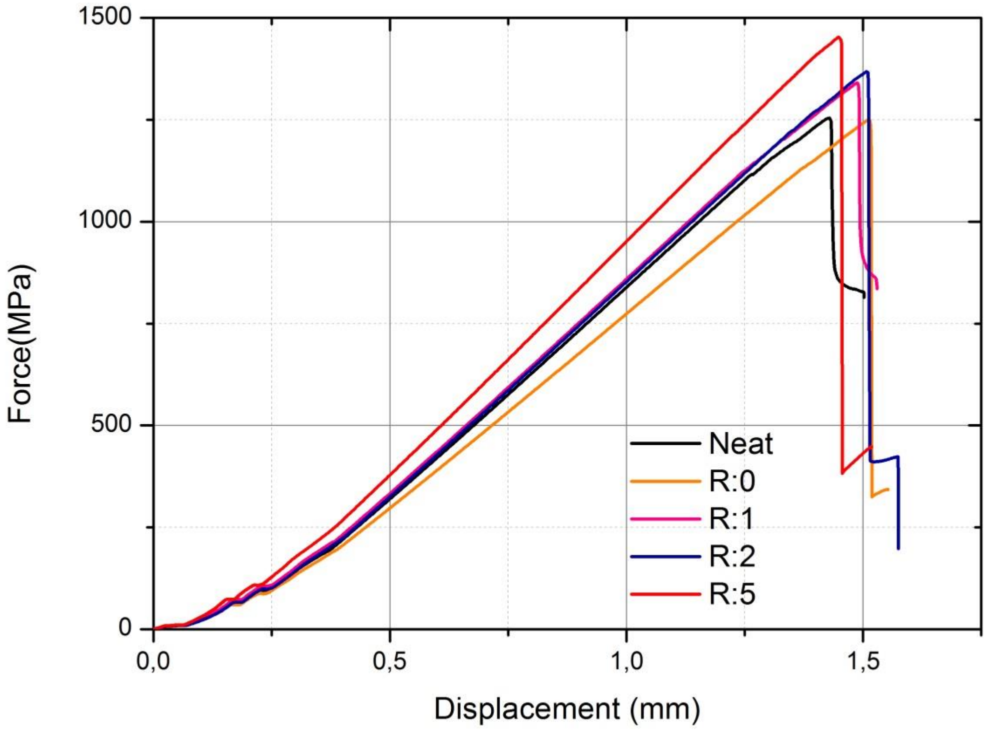

Figure 3.8: Representative 3-Point Bending test curves for $(0)_3$ laminates

As shown in the figure 3.8 the addition of the P(St-co-GMA)/PA-TBA nanofibers to the laminated composites with an increasing PA/GMA ratio led to increase in flexural properties in the same manner up to 15%, while P(St-co-GMA) nanofiber introduced laminates' flexural properties diminish compared to the neat laminates when cured at above Tg temperatures. However the earlier works of the group revealed that P(St-co-GMA) nanofiber addition of the system at lower curing temperatures than the nanofiber' glass transition point led to an increase at the flexural properties[1, 6-8].

Table 3.4: 3-Point Bending test results

PA/GMA ratio of interlayer	Flexural Strength (MPa)
Neat	1254
R:0	1340
R:1	1340
R:2	1368
R:5	1452

It can be expected that two distinct failure mechanisms, transverse matrix cracking and/or delamination cause to failure in $(0)_3$ laminates. It is known that the co-existence of these two mechanisms enable the creation of pure shear conditions via 3-point bending tests [6]. The representative failure modes are given in the figure 3.9. The flexural strength increase reported via 3-point bending tests characterized both resistance to delamination and matrix toughening by the addition of the nanofibrous interlayers. Pure shear conditions are also observed by ENF tests done[30].

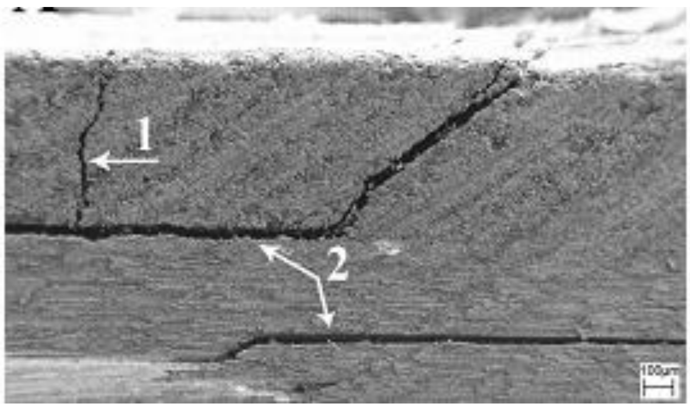

Figure 3.9: Representative cross-sectional view for fractured 3-point bending specimens both include transverse matrix cracking (1) and delamination (2)

3.3.4 Mode II Strain Energy release rate by ENF Tests

Heat Stimuli-Self-Crosslinked interlayer at the pre-crack tip increased G_{IIC} by 80% whereas the interlayers of P(St-co-GMA) nanofibers decreased G_{IIC} by 40% since the curing temperature of the composites was higher than their glass transition temperature (135 C for 2 hours). It should be noted that the earlier works of the group showed that for curing cycles at lower temperature for longer time (100 C for 8 hours) P(St-co-GMA) nanofibers did not transform and were as successful leading to increase at mode II strain energy release rate by about 55 %.

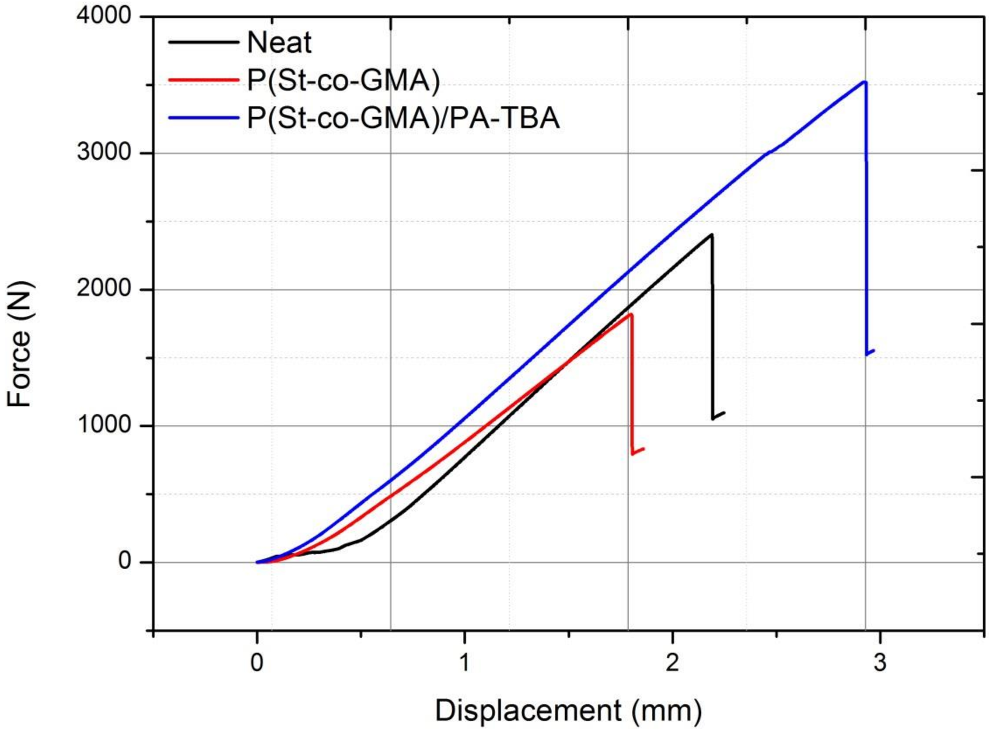

Figure 3.10: Representative ENF test curves for $(0)_{48}$ laminates

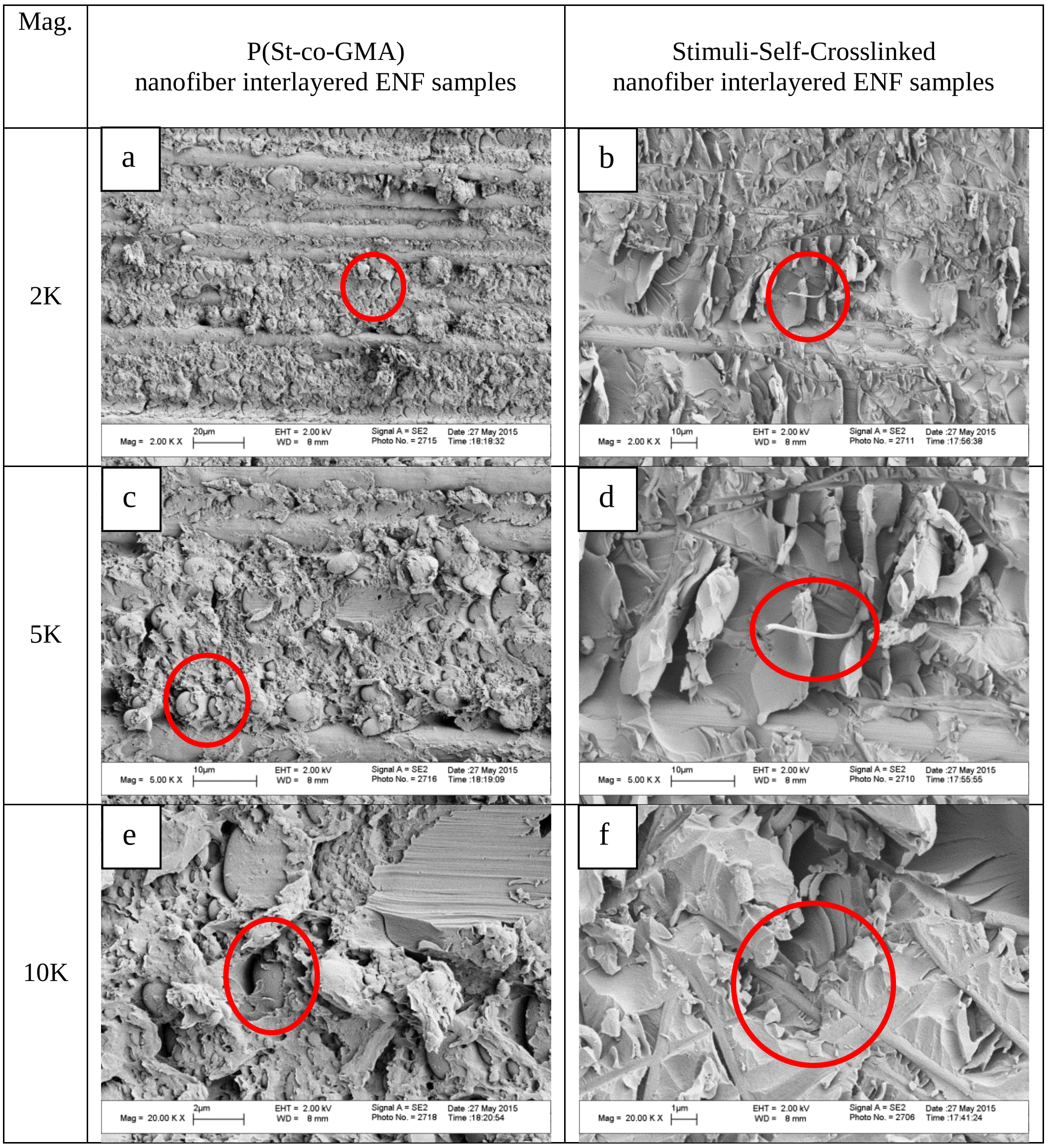

Figure 3.11: Fracture surfaces of P(St-co-GMA) and Stimuli-Self crosslinked Nanofiber interlayered interface. Zoomed in views for encircled areas for each interlayer. (Magnifications: 500, 1K, 5K)

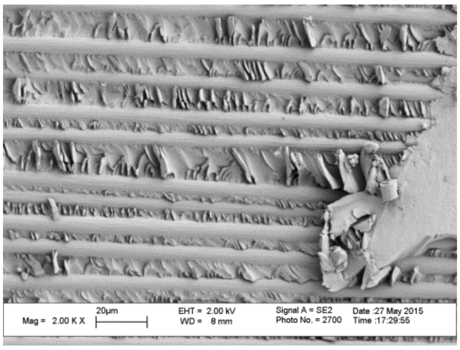

Figure 3.12: Fracture surfaces of neat interface

Failure of ENF specimens was observed as dominated by unstable crack growth parallel to the interlaminar plane with a drastic load drop. UD laminates, under the ENF test configurations with constant displacement rate, exhibit unstable crack growth that can arguably be considered as an inherent characteristic of the test conditions[50],[6]. Further morphologic analysis of the fracture surfaces also suggested that the G_{IIC} enhancement was directly associated with the active role of crosslinked interlayers on the resistance to fracture. The hackle patterns for the neat laminate without the interlayers (figure 3.12) are conclusive. They are typically formed due to the micro-crack coalescence as clearly distinguishable all along the crack path[51]. However the hackle patterns for the interlayered laminates had different characteristics, by more complex structures, they are enlarged or deteriorated by the nanofibers' morphological changes (see figure 3.11). Pulled out nanofibers in Figure 3.11 (b,d,f) indicate their superior mechanical strength and higher energy to develop fracture/crack growth.

3.4 Concluding Remarks

Nanofibrous heat stimuli-self-crosslinkable P(St-co-GMA)/PA-TBA interlayers were deposited on carbon/epoxy prepreg surfaces. P(St-co-GMA) nanofiber interlayers were used as reference to highlight the effect of corsslinking within the fibers. Composite laminates were produced by curing at high temperature (higher than the glass transition temperature of the P(St-co-GMA) nanofibers) and short dwell time. Consequently a homogeneous crosslinking regime was obtained through the nanofibers itself and between the interlayers and epoxy matrix. 3-point bending test results reveal that 15% increase at the flexural strength can be obtained. The mode II delamination resistance was increased up to %80 attributed to noticeable fracture pattern changes which require more energy due to existence of Nanofibrous interlayers. They were incorporated into the structural composites due to the additional chemical bonds between nanofibers itself and between epoxy matrix and nanofibers. This suggested structural compatibility could also be attributed as an explanation for resistance against matrix cracking.

REFERENCES

[1] Ozden E, Menceloglu YZ, Papila M. Engineering chemistry of electrospun nanofibers and interfaces in nanocomposites for superior mechanical properties. ACS applied materials & interfaces 2010;2:1788-93.

[2] Huang Z-M, Zhang Y-Z, Kotaki M, Ramakrishna S. A review on polymer nanofibers by electrospinning and their applications in nanocomposites. Composites science and technology 2003;63:2223-53.

[3] Özden-Yenigün E, Menceloğlu YZ, Papila M. MWCNTs/P (St-co-GMA) composite nanofibers of engineered interface chemistry for epoxy matrix nanocomposites. ACS applied materials & interfaces 2012;4:777-84.

[4] Zong X, Kim K, Fang D, Ran S, Hsiao BS, Chu B. Structure and process relationship of electrospun bioabsorbable nanofiber membranes. Polymer 2002;43:4403-12.

[5] Zucchelli A, Focarete ML, Gualandi C, Ramakrishna S. Electrospun nanofibers for enhancing structural performance of composite materials. Polymers for Advanced Technologies 2011;22:339-49.

[6] Bilge K, Ozden-Yenigun E, Simsek E, Menceloglu Y, Papila M. Structural composites hybridized with epoxy compatible polymer/MWCNT nanofibrous interlayers. Composites Science and Technology 2012;72:1639-45.

[7] Bilge K, Özden Yenigün E, Şimşek E, Menceloğlu YZ, Papila M. Strength of hybrid composites reinforced with surface modified polymer/MWCNTs nano-composite interlayers. 2011.

[8] Bilge K, Venkataraman S, Menceloglu Y, Papila M. Global and local nanofibrous interlayer toughened composites for higher in-plane strength. Composites Part A: Applied Science and Manufacturing 2014;58:73-6.

[9] Zheng J, He A, Li J, Xu J, Han CC. Studies on the controlled morphology and wettability of polystyrene surfaces by electrospinning or electrospraying. Polymer 2006;47:7095-102.

[10] Yördem O, Papila M, Menceloğlu YZ. Effects of electrospinning parameters on polyacrylonitrile nanofiber diameter: An investigation by response surface methodology. Materials & design 2008;29:34-44.

[11] Dai T, Ebert K. Electrospinning of solvent-resistant nanofibers based on poly(acrylonitrile-co-glycidyl methacrylate). Journal of Applied Polymer Science 2012;126:136-42.

[12] Peresin MS, Vesterinen AH, Habibi Y, Johansson LS, Pawlak JJ, Nevzorov AA, et al. Crosslinked PVA nanofibers reinforced with cellulose nanocrystals: Water

interactions and thermomechanical properties. Journal of Applied Polymer Science 2014;131.

[13] Gupta P, Trenor SR, Long TE, Wilkes GL. In situ photo-cross-linking of cinnamate functionalized poly (methyl methacrylate-co-2-hydroxyethyl acrylate) fibers during electrospinning. Macromolecules 2004;37:9211-8.

[14] Kim SH, Kim S-H, Nair S, Moore E. Reactive electrospinning of cross-linked poly (2-hydroxyethyl methacrylate) nanofibers and elastic properties of individual hydrogel nanofibers in aqueous solutions. Macromolecules 2005;38:3719-23.

[15] Ji Y, Ghosh K, Li B, Sokolov JC, Clark RA, Rafailovich MH. Dual-Syringe Reactive Electrospinning of Cross-Linked Hyaluronic Acid Hydrogel Nanofibers for Tissue Engineering Applications. Macromolecular bioscience 2006;6:811-7.

[16] Stone SA, Gosavi P, Athauda TJ, Ozer RR. In situ citric acid crosslinking of alginate/polyvinyl alcohol electrospun nanofibers. Materials Letters 2013;112:32-5.

[17] Liu H, Zhen M, Wu R. Ionic-Strength-and pH-Responsive Poly [acrylamide-co-(maleic acid)] Hydrogel Nanofibers. Macromolecular Chemistry and Physics 2007;208:874-80.

[18] Tang C, Saquing CD, Harding JR, Khan SA. In SituCross-Linking of Electrospun Poly(vinyl alcohol) Nanofibers. Macromolecules 2010;43:630-7.

[19] Matějka L, Lövy J, Pokorný S, Bouchal K, Dušek K. Curing epoxy resins with anhydrides. Model reactions and reaction mechanism. Journal of Polymer Science: Polymer Chemistry Edition 1983;21:2873-85.

[20] Fischer RF. Polyesters from Epoxides and Anhydrides. JOURNAL OF POLYMER SCIENCE 1960;44:155-72.

[21] Antoon MK, Koenig JL. Crosslinking mechanism of an anhydride-cured epoxy resin as studied by fourier transform infrared spectroscopy. Journal of Polymer Science: Polymer Chemistry Edition 1981;19:549-70.

[22] Tillet G, Boutevin B, Ameduri B. Chemical reactions of polymer crosslinking and post-crosslinking at room and medium temperature. Progress in Polymer Science 2011;36:191-217.

[23] Kim K-J, Lee S-B, Han N-W. Kinetics of crosslinking reaction of PVA membrane with glutaraldehyde. Korean Journal of Chemical Engineering 1994;11:41-7.

[24] Guerrero P, De la Caba K, Valea A, Corcuera M, Mondragon I. Influence of cure schedule and stoichiometry on the dynamic mechanical behaviour of tetrafunctional epoxy resins cured with anhydrides. Polymer 1996;37:2195-200.

[25] Luo X, Zheng S, Ma D. Mechanical Relaxation and Intermolecular Interaction in Epoxy Resins/ (Poly Ethylene Oxide) Blends Cured with Phthalic Anhydride. Chinese Journel of Polymer Science 1995;13:144-53.

[26] Romão BMV, Diniz MF, Azevedo MFP, Lourenço VL, Pardini LC, Dutra RCL, et al. Characterization of the Curing Agents Used in Epoxy Resins with TG/FT-IR Technique. Polímeros: Ciência e Tecnologia 2006;16:94-8.

[27] Kim Js, Reneker DH. Mechanical properties of composites using ultrafine electrospun fibers. Polymer composites 1999;20:124-31.

[28] Tsotsis TK. Interlayer toughening of composite materials. Polymer Composites 2009;30:70-86.

[29] Dzenis YA, Reneker DH. Delamination resistant composites prepared by small diameter fiber reinforcement at ply interfaces. Google Patents; 2001.

[30] Sihn S, Kim RY, Huh W, Lee K-H, Roy AK. Improvement of damage resistance in laminated composites with electrospun nano-interlayers. Composites Science and Technology 2008;68:673-83.

[31] Liu L, Huang Z-M, He C, Han X. Mechanical performance of laminated composites incorporated with nanofibrous membranes. Materials Science and Engineering: A 2006;435:309-17.

[32] Liu L, Huang ZM, Xu GY, Liang YM, Dong GH. Mode II interlaminar delamination of composite laminates incorporating with polymer ultrathin fibers. Polymer Composites 2008;29:285-92.

[33] Lee S-H, Lee J-H, Cheong S-K, Noguchi H. A toughening and strengthening technique of hybrid composites with non-woven tissue. journal of materials processing technology 2008;207:21-9.

[34] Lee S-H, Noguchi H, Kim Y-B, Cheong S-K. Effect of interleaved non-woven carbon tissue on interlaminar fracture toughness of laminated composites: Part I–Mode II. Journal of composite materials 2002;36:2153-68.

[35] Palazzetti R, Zucchelli A, Gualandi C, Focarete M, Donati L, Minak G, et al. Influence of electrospun Nylon 6, 6 nanofibrous mats on the interlaminar properties of Gr–epoxy composite laminates. Composite Structures 2012;94:571-9.

[36] Magniez K, Chaffraix T, Fox B. Toughening of a carbon-fibre composite using electrospun poly (hydroxyether of bisphenol a) nanofibrous membranes through inverse phase separation and inter-domain etherification. Materials 2011;4:1967-84.

[37] Zhang J, Lin T, Wang X. Electrospun nanofibre toughened carbon/epoxy composites: Effects of polyetherketone cardo (PEK-C) nanofibre diameter and interlayer thickness. Composites science and technology 2010;70:1660-6.

[38] Zhang J, Yang T, Lin T, Wang CH. Phase morphology of nanofibre interlayers: Critical factor for toughening carbon/epoxy composites. Composites science and technology 2012;72:256-62.

[39] Bortz DR, Merino C, Martin-Gullon I. Mechanical characterization of hierarchical carbon fiber/nanofiber composite laminates. Composites Part A: Applied Science and Manufacturing 2011;42:1584-91.

[40] Arai M, Sasaki T, Hirota S, Ito H, Hu N, Quaresimin M. Mixed modes interlaminar fracture toughness of CFRP laminates toughened with CNF interlayer. Acta Mechanica Solida Sinica 2012;25:321-30.

[41] Bortz DR, Merino C, Martin-Gullon I. Carbon nanofibers enhance the fracture toughness and fatigue performance of a structural epoxy system. Composites Science and Technology 2011;71:31-8.

[42] Zainuddin S, Mahfuz H, Jeelani S. Enhancing fatigue performance of sandwich composites with nanophased core. Journal of Nanomaterials 2010;2010:11.

[43] Grimmer CS, Dharan C. High-cycle fatigue of hybrid carbon nanotube/glass fiber/polymer composites. Journal of Materials Science 2008;43:4487-92.

[44] Zhou Y, Pervin F, Jeelani S, Mallick P. Improvement in mechanical properties of carbon fabric–epoxy composite using carbon nanofibers. Journal of materials processing technology 2008;198:445-53.

[45] Manjunatha C, Taylor A, Kinloch A, Sprenger S. The tensile fatigue behaviour of a GFRP composite with rubber particle modified epoxy matrix. Journal of reinforced Plastics and Composites 2009.

[46] Manjunatha C, Sprenger S, Taylor A, Kinloch A. The tensile fatigue behavior of a glass-fiber reinforced plastic composite using a hybrid-toughened epoxy matrix. Journal of composite materials 2010;44:2095-109.

[47] Manjunatha C, Taylor A, Kinloch A, Sprenger S. The tensile fatigue behaviour of a silica nanoparticle-modified glass fibre reinforced epoxy composite. Composites Science and Technology 2010;70:193-9.

[48] Rafiee MA, Rafiee J, Srivastava I, Wang Z, Song H, Yu ZZ, et al. Fracture and fatigue in graphene nanocomposites. small 2010;6:179-83.

[49] Albertsen H, Ivens J, Peters P, Wevers M, Verpoest I. Interlaminar fracture toughness of CFRP influenced by fibre surface treatment: Part 1. Experimental results. Composites Science and Technology 1995;54:133-45.

[50] Seyhan AT, Tanoglu M, Schulte K. Mode I and mode II fracture toughness of E-glass non-crimp fabric/carbon nanotube (CNT) modified polymer based composites. Engineering Fracture Mechanics 2008;75:5151-62.

[51] Stevanovic D, Kalyanasundaram S, Lowe A, Jar P-Y. Mode I and mode II delamination properties of glass/vinyl-ester composite toughened by particulate modified interlayers. Composites science and technology 2003;63:1949-64.